Article

Comparison of Experimental *vs.* Theoretical Abundances of CHD and CHD for Isotopically Equilibrated Systems From 1-500°C

Daniel Lee Eldridge, Roman Korol, Max K. Lloyd, Andrew C. Turner, Michael A Webb, Thomas Francis Miller, and Daniel Stolper

ACS Earth Space Chem., **Just Accepted Manuscript** • DOI: 10.1021/acsearthspacechem.9b00244 • Publication Date (Web): 28 Oct 2019

Comparison of Experimental *vs.* Theoretical Abundances of $^{13}CH_3D$ and $^{12}CH_2D_2$ for Isotopically Equilibrated Systems From 1-500°C

Daniel L. Eldridge*[1,2], Roman Korol[3], Max K. Lloyd[2], Andrew C. Turner[2], Michael A. Webb[4], Thomas F. Miller III[3], Daniel A. Stolper[1,2]

[1]*Energy Geosciences Division, Lawrence Berkeley National Laboratory, 1 Cyclotron Road, Berkeley, CA 94720 USA*
[2]*Department of Earth and Planetary Science, University of California, Berkeley, CA 94720 USA*
[3]*Division of Chemistry and Chemical Engineering, California Institute of Technology, Pasadena, CA 91125 USA*
[4]*Department of Chemical and Biological Engineering, Princeton University, Princeton, New Jersey 08544 USA*

*To whom correspondence should be addressed: danieleldridge@lbl.gov

Abstract

Methane is produced and consumed *via* numerous microbial and chemical reactions in atmospheric, hydrothermal, and magmatic reactions. The stable isotopic composition of methane has been used extensively for decades to constrain the source of methane in the environment. A recently introduced isotopic parameter used to study the formation temperature and formational conditions of methane is the measurement of molecules of methane with multiple rare, heavy isotopes ('clumped') such as $^{13}CH_3D$ and $^{12}CH_2D_2$. In order to place methane clumped-isotope measurements into a thermodynamic reference frame that allows calculations of clumped-isotope based temperatures (geothermometry) and comparison between laboratories, all past studies have calibrated their measurements using a combination of experiment and theory based on the temperature dependence of clumped isotopologue distributions for isotopically equilibrated systems. These have previously been performed at relatively high temperatures (>150˚C). Given that many natural occurrences of methane form below these temperatures, previous calibrations require extrapolation when calculating clumped-isotope based temperatures outside of this calibration range. We provide a new experimental calibration of the relative equilibrium abundances of $^{13}CH_3D$ and $^{12}CH_2D_2$ from 1–500˚C using a combination of γ-Al_2O_3 and Ni-based catalysts and compare them to new theoretical computations using Path Integral Monte Carlo (PIMC) methods and find 1:1 agreement (within ±1 standard error) for the observed temperature dependence of clumping between experiment and theory over this range. This demonstrates that measurements, experiments, and theory agree from 1–500°C providing confidence in the overall approaches. Polynomial fits to PIMC computations, which are considered the most rigorous theoretical approach available, are given as follows (valid $T \geq 270$ K):

$$\Delta_{^{13}CH_3D} \cong 1000 \times \ln\left(K_{^{13}CH_3D}\right) = \frac{1.47348 \times 10^{19}}{T^7} - \frac{2.08648 \times 10^{17}}{T^6} + \frac{1.19810 \times 10^{15}}{T^5} - \frac{3.54757 \times 10^{12}}{T^4} + \frac{5.54476 \times 10^{9}}{T^3} - \frac{3.49294 \times 10^{6}}{T^2} + \frac{8.89370 \times 10^{2}}{T}$$

$$\Delta_{^{12}CH_2D_2} \cong 1000 \times \ln\left(\frac{8}{3}K_{^{12}CH_2D_2}\right) = -\frac{9.67634 \times 10^{15}}{T^6} + \frac{1.71917 \times 10^{14}}{T^5} - \frac{1.24819 \times 10^{12}}{T^4} + \frac{4.30283 \times 10^{9}}{T^3} - \frac{4.48660 \times 10^{6}}{T^2} + \frac{1.86258 \times 10^{3}}{T}.$$

We additionally compare PIMC computations to those performed utilizing traditional approaches that are the basis of most previous calibrations (Bigeleisen, Mayer, and Urey model, BMU) and discuss the potential sources of error in the BMU model relative to PIMC computations.

Keywords: Methane Clumped Isotopes, Methane Isotope Equilibration, Methane Geochemistry, Path Integral Monte Carlo Calculations, 253 Ultra

1. Introduction

Methane is a product and reactant in atmospheric, hydrothermal, and magmatic chemical reactions and in microbial metabolisms. It is also a major component of commercial hydrocarbon deposits. A common first step in the study of methane in the environment, regardless of the application, is to constrain its source. A long-standing approach for this is to use the stable isotopic composition of a methane sample either through comparison of methane $^{13}C/^{12}C$ vs. D/H ratios to each other (given as $\delta^{13}C$ and δD values†; e.g., refs[1,2]), to the concentration of alkanes gases (e.g., methane, ethane propane, and butane; e.g., ref[3]), or to the stable isotopic composition of larger alkane gases (e.g., ref[4]).

The measurement of molecules of methane with multiple rare, heavy ('clumped') isotopes such as $^{13}CH_3D$ and $^{12}CH_2D_2$ has provided a new way to study the formational conditions of methane.[5–7] For an isotopically equilibrated system, the abundance of these clumped isotopologues relative to that expected for a random distribution of isotopes among all methane molecules is a monotonic function of temperature[5–11]. Thus, the measurement of methane clumped-isotope compositions (relative to a random isotopic distribution) can in principle be used as a geothermometer and to study departures of samples from isotopic equilibrium. Applications of methane clumped-isotope studies include the determination of apparent formation (or re-equilibration) temperatures of methane in subsurface reservoirs and to fingerprint abiotic, biogenic, and thermogenic methane.[7,12,21,22,13–20]

These capabilities arise from the ability to precisely measure (order per mil) the relative abundances of unsubstituted ($^{12}CH_4$), singly substituted ($^{12}CH_3D$, $^{13}CH_4$) and multiply substituted isotopologues of methane ($^{13}CH_3D$,$^{12}CH_2D_2$) using either high-resolution gas-source isotope-ratio mass spectrometers (e.g., refs[5,7,23,24]) or laser absorption spectrometers[6]. Regardless of the technique, measurements are performed relative to commercial high-purity methane 'working gases', which have *a priori* unknown clumped-isotope compositions. As a result, measured methane clumped-isotope compositions are not inherently anchored to an external reference frame such as one set by international standards (which are not available) or set by theoretical expectations of the equilibrium temperature dependence of methane clumping. Past studies have combined experiment and theory to place measured clumped-isotope compositions into a reference frame anchored by theoretical expectations of the equilibrium temperature dependence of $^{13}CH_3D$ or $^{12}CH_2D_2$ concentrations *vs.* their expected concentrations for a system in isotopic equilibrium with a random distribution of isotopes[5–7,14]. To accomplish this, previous studies isotopically equilibrated methane isotopologues at temperatures greater than 150°C in the presence of catalysts that promote C-H bond activation and hydrogen isotope exchange. The measured differences between samples equilibrated at different temperatures were then compared to statistical mechanical-based theoretical calculations of these expected differences (e.g., refs[5–7]). All

† $\delta D_{VSMOW} = ({}^{D}R_{wg}/{}^{D}R_{VSMOW} - 1)\times 1000$ and $\delta^{13}C_{VPDB} = ({}^{13}R_{wg}/{}^{13}R_{VPDB} - 1)\times 1000$; ${}^{D}R = [D]/[H]$ and ${}^{13}R = [{}^{13}C]/[{}^{12}C]$

measurements of clumped methane compositions are based on this approach and are performed on a lab-by-lab basis. The accuracy of such 'heated gas' calibrations and thus measured methane clumped-isotope compositions and apparent temperatures depends on the accuracy of the theoretical calculations, the experiments, and the isotopic measurements.

1.1 Isotope-exchange reactions and nomenclature

Two clumped methane isotopologues ($^{13}CH_3D$ and $^{12}CH_2D_2$) have been measured at precisions necessary to calculate clumped-isotope based temperatures at useful precisions (± <25˚C) at temperatures < 200°C for samples with natural abundances of stable isotopes. The abundances of these species for a given measurement are reported using Δ notation[25] such that:

$$\Delta_{^{13}CH_3D} = 1000 \times \left(\frac{[^{13}CH_3D]/[^{12}CH_4]}{[^{13}CH_3D]^*/[^{12}CH_4]^*} - 1 \right) \quad (1)$$

and

$$\Delta_{^{12}CH_2D_2} = 1000 \times \left(\frac{[^{12}CH_2D_2]/[^{12}CH_4]}{[^{12}CH_2D_2]^*/[^{12}CH_4]^*} - 1 \right). \quad (2)$$

In Eq. 1 and 2, the brackets denote concentrations relative to all other methane isotopologues and the * denotes the calculated concentration of an isotopologue assuming all isotopes of carbon and hydrogen are randomly distributed among all isotopologues (see ref[25] for a more detailed review). These Δ values can be related to the following isotope-exchange reactions:

$$^{13}CH_4 + {}^{12}CH_3D \rightleftharpoons {}^{12}CH_4 + {}^{13}CH_3D \quad (3)$$

and

$$2\,{}^{12}CH_3D \rightleftharpoons {}^{12}CH_4 + {}^{12}CH_2D_2\,. \quad (4)$$

$K_{^{13}CH_3D}$ and $K_{^{12}CH_2D_2}$ describe the equilibrium constants for Eq. 3 and 4, respectively.

For isotopically equilibrated systems, Δ and K values are related through the following equations (see derivation in ref[25]):

$$\Delta_{^{13}CH_3D} \cong 1000 \times \ln(K_{^{13}CH_3D}) \quad (5)$$

and

$$\Delta_{^{12}CH_2D_2} \cong 1000 \times \ln\left(\frac{8}{3} K_{^{12}CH_2D_2}\right) \quad (6)$$

The 8/3 value is present in Eq. 6 due to the differing symmetry numbers of the various methane isotopologues in Eq. 4. The approximate signs are present because we assume that the concentrations of the $^{13}CH_4$ and $^{12}CH_3D$ isotopologues are equal to values expected for a random isotopic distribution. This is only approximately true, but as discussed in ref[5], this approximation is valid for our purposes given both the measurement precisions (±1 s.e.) that will be reported below for $\Delta_{^{13}CH_3D}$ (±0.25-0.3‰) and $\Delta_{^{12}CH_2D_2}$ (±1-1.5‰) as well as typical $\delta^{13}C$ and δD ranges of environmental samples (~70 and ~500‰, respectively).

We note that an additional parameter that was used for the first methane clumped isotope measurements is Δ_{18}.[5] This represents the combined measurements of $^{13}CH_3D$ and $^{12}CH_2D_2$ *vs.* $^{12}CH_4$ compared to a random isotopic distribution (see ref[5]). Δ_{18} values are largely equivalent to

$\Delta_{^{13}CH_3D}$ values because 98% of the cardinal mass-18 methane isotopologues are $^{13}CH_3D$ and 2% are $^{12}CH_2D_2$.

The key point for our purposes here is that the measured Δ quantities are directly related to temperature-dependent equilibrium isotope-exchange reactions for isotopically equilibrated systems (i.e., in homogeneous phase equilibrium). Thus, if samples can be isotopically equilibrated at known temperatures and the theoretically expected differences calculated, then the Δ value of samples can be converted into apparent temperatures based on well-understood quantum-statistical-mechanical theories regardless of the clumped-isotopic composition of the reference gas used during measurements.

1.2 Previous experimental and theoretical determinations of the temperature dependence of Δ values for isotopically equilibrated systems

Experimental calibrations and temperature dependencies of $\Delta_{^{13}CH_3D}$ and $\Delta_{^{12}CH_2D_2}$ for isotopically equilibrated systems have been conducted at temperatures above 150˚C[14] and 300°C[7], respectively, and above 200˚C for Δ_{18} values[5]. In contrast, formation temperatures of biogenic gases on earth are typically thought to be below 80°C (e.g., refs[26,27]) while thermogenic gases are thought to begin forming as low as 60°C[28]. Thus, the potential range of expected gas-formation temperatures in nature is commonly outside of these calibrated ranges. This requires extrapolation of calibrations to lower temperatures and higher Δ values to calculate clumped-isotope based temperatures. Stolper and co-workers[5] calibrated equilibrium Δ_{18} values at four temperatures (200, 300, 400, and 500˚C) using a nickel-based catalyst that represented a total measured range in Δ_{18} of 1.8‰ (quoted internal precision of ±0.25-0.3‰, ±1 s.e. and external precision of ±0.25-0.3‰, ±1σ). Following this, Ono and co-workers[6] calibrated equilibrium $\Delta_{^{13}CH_3D}$ values at three temperatures (200, 300, and 400˚C) using a platinum-based catalyst that represented a total measured range in $\Delta_{^{13}CH_3D}$ of about 1.4‰ (quoted ±1σ internal precision of ±0.1‰, and external ±1σ precision of ±0.35‰; note the external precision incorporates both reproducibility and accuracy; σ = standard deviation). In the same laboratory, Wang and co-workers[14] performed a similar calibration using a platinum catalyst at three temperatures (150, 170, and 250˚C) and a total measured range in $\Delta_{^{13}CH_3D}$ of about 1.2‰. They[14] additionally measured a sample at 400°C, but this data point was not included in their calibration because it did not fit with the expected theoretical temperature dependence. It was proposed that the sample may have been compromised by potential quench effects. Finally, Young and co-workers[7] calibrated equilibrium $\Delta_{^{13}CH_3D}$ and $\Delta_{^{12}CH_2D_2}$ values at three temperatures (300, 400, and 500˚C) using a platinum-based catalyst representing a total measured range in $\Delta_{^{13}CH_3D}$ of 1.0‰ and $\Delta_{^{12}CH_2D_2}$ of about 2.2‰ (quoted internal ±1 s.e. precision ±0.15‰ and ±0.35‰, respectively). The external precision (± 1σ; note this incorporates both reproducibility and accuracy) of these measurements from the same lab was stated to be ±0.3‰ and ±1.0‰ for $\Delta_{^{13}CH_3D}$ and $\Delta_{^{12}CH_2D_2}$, respectively, in ref[12].

The lack of samples equilibrated at temperatures <150°C, despite expectations that biogenic and thermogenic gases could form at such temperatures, is due to the usage of catalysts (nickel- and platinum-based) that do not facilitate reaction at temperatures <150°C over laboratory timescales. For example, the calibration of the equilibrium value for $\Delta_{^{13}CH_3D}$ at 150˚C (representing the lowest

clumped methane calibration temperature reported in the above studies) is based on a single experiment that was allowed to react/equilibrate for 110 days.[14] The ability to extend calibrations to lower temperatures using methane equilibrated in the laboratory would allow for more detailed comparisons between theory and experiment and allow apparent clumped-isotope based temperatures to be calculated based on interpolation of calibrations as opposed to extrapolations.

Previous theoretical calculations of equilibrium $\Delta_{^{13}CH_3D} \cong 1000 \times \ln(K_{^{13}CH_3D})$ and $\Delta_{^{12}CH_2D_2} \cong 1000 \times \ln\left(\frac{8}{3}K_{^{12}CH_2D_2}\right)$ values are based on one of two theoretical approaches: (*i*) The Bigeleisen and Mayer/Urey model[29,30] (BMU; e.g., refs[7–10,14,31]), which in practice involves calculations of so-called reduced partition function ratios (RPFRs) using a harmonic approximation for the treatment of the vibrational partition function and classical expressions for rotational and translational partition functions; and (*ii*) Path Integral Monte Carlo (PIMC) simulations that avoid the major approximations in the BMU model yielding a fully anharmonic and quantum mechanical description of the partition function ratios[11].

Both approaches require independent computations of the electronic potential energy surface for methane, which are typically taken from electronic structure calculations based on density functional theory (DFT) or more accurate *ab initio* wavefunction theories, such as coupled-cluster theory. Differences in previous theoretical calculations of equilibrium $\Delta_{^{13}CH_3D}$ values given as $1000 \times \ln(K_{^{13}CH_3D})$ as a function of temperature based on the BMU model using harmonic frequencies are comparable to the typical internal precision of $\Delta_{^{13}CH_3D}$ measurements (≤ 0.2‰ for $T \geq 0$˚C; e.g., refs[8–10]). Cao and Liu[31] initially assessed the effect of *ex post facto* anharmonic corrections to $\Delta_{^{13}CH_3D}$ and found deviations (up to ~0.2‰) that are comparable to typical internal precision of $\Delta_{^{13}CH_3D}$ measurements. A later study[9] from the same group applied a series of *ex post facto* corrections to harmonic RPFRs to account for the effects of anharmonicity and many of the other major approximations inherent to the BMU model using computed isotopologue-specific molecular constants following approaches summarized in refs[32,33]. In this study[9], smaller differences were found in computed $\Delta_{^{13}CH_3D}$ values given as $1000 \times \ln(K_{^{13}CH_3D})$ relative to uncorrected values based on harmonic RPFRs but the differences may be systematic in nature (i.e., +0.04‰ at 0˚C to +0.07‰ at 500˚C).

Webb and Miller[11] performed theoretical calculations of $\Delta_{^{13}CH_3D}$ values given as $1000 \times \ln(K_{^{13}CH_3D})$ using both PIMC and BMU approaches (with and without anharmonic corrections for the BMU approach) based on the same computed electronic potential energy surface[34] for all calculations from 27-327°C. Calculations of $\Delta_{^{13}CH_3D}$ values using both PIMC and BMU-harmonic approaches yielded similar results over the temperature ranges studied (i.e., all are within ≤ 0.06‰ over 27-327˚C). However, they[11] illustrated that the apparent agreement between the BMU-harmonic and PIMC calculations arises due to a precise cancelation of errors in the harmonically computed RPFRs during computation of the equilibrium constant. They[11] further demonstrated that an *ex post facto* anharmonic correction to the vibrational zero point energy resulted in comparatively worse agreement (e.g., 0.2-0.4‰ differences in $\Delta_{^{13}CH_3D}$ relative to PIMC[11]). It is important to note that precise error cancelation between PFRs was not universally observed by Webb and Miller[11]. For example, in the isotope-exchange reaction describing position-specific isotope abundances for isotopically equilibrated system between $^{14}N^{15}N^{16}O$ and $^{15}N^{14}N^{16}O$, an

anharmonic correction did yield overall better agreement with PIMC results. This indicates that the partial corrections to the BMU model may or may not improve accuracy of results.

Theoretical calculations of equilibrium $\Delta_{^{12}CH_2D_2}$ values as given by $1000 \times \ln\left(\frac{8}{3}K_{^{12}CH_2D_2}\right)$ as a function of temperature have been performed in two studies based solely on the harmonic BMU model[7,10]. The calculated $\Delta_{^{12}CH_2D_2}$ values from these two studies as a function of temperature are similar (differ ≤ 0.44‰ for temperatures ≥ 0°C).

1.3 This study

Here, we provide an experimental calibration of equilibrium $\Delta_{^{13}CH_3D}$ and $\Delta_{^{12}CH_2D_2}$ values from 1-500˚C and compare this calibration to new theoretical computations of equilibrium $\Delta_{^{13}CH_3D}$ and $\Delta_{^{12}CH_2D_2}$values as a function of temperature using PIMC methods[11,35] and BMU calculations based on the same electronic potential energy surface to facilitate direct comparison. To achieve isotopic equilibrium on laboratory time scales, we use a γ-Al_2O_3 catalyst to equilibrate methane from 1-165˚C and a nickel-based catalyst for higher temperatures (250-500˚C). We then compare these results to the expected differences using different theoretical approaches for computing clumped methane compositions (i.e., PIMC and BMU). We show that the theoretical and experimental measurements are in 1:1 agreement from 1-500°C and thus provide a calibration for the relative equilibrium abundances of both $^{13}CH_3D$ and $^{12}CH_2D_2$ over this temperature range validated by both experiment and theory.

This work including experimental techniques was originally described and presented in two abstracts[36,37]. Following presentation of this work and during the drafting of this manuscript, we became aware that Wang et al. (accepted)[38] also recently used γ-Al_2O_3 catalysts to equilibrate $\Delta_{^{13}CH_3D}$ values of methane at 25 and 100°C, though using a different approach. Their total measured $\Delta_{^{13}CH_3D}$ range is 1.90‰ with analytical precisions of generally ±1‰ (95% confidence interval).[38] Both their and our success in equilibrating $\Delta_{^{13}CH_3D}$ using this catalyst demonstrates its general ability to equilibrate methane clumped-isotopic compositions at low (<150°C) temperatures.

2. Methods

2.1 House methane 'working gas', in-house standards, and calibration to VSMOW and VPDB

All methane used in this study was prepared from a single tank of 99.999% pure compressed methane (5.0 Research grade; Praxair). This gas is referred to as either the 'house methane' in the context of experimental preparation or the 'working gas' (wg) in the context of mass spectrometric measurements. Internal reference standards having higher δD, $\delta^{13}C$, or $\Delta_{^{12}CH_2D_2}$ values than the house methane were prepared by adding labeled methane to 500 ml glass bottles filled with ~1 atm of the house methane. Specifically, $^{12}CH_3D$ (98 atom % D; Sigma Aldrich), $^{13}CH_4$ (99 atom % ^{13}C; Sigma Aldrich), or $^{12}CH_2D_2$ (98 atom % D; Sigma Aldrich) were added to the house methane to make internal standards with the desired isotopic compositions.

The δD and $\delta^{13}C$ values of the house methane and internal in-house standards were independently determined at the Stable Isotope Facility in the Department of Plant Sciences at UC Davis (SIF-UCD) using standard combustion and pyrolysis techniques previously described[39].

2.2 Equilibrated gas experiments

2.2.1 γ-Al_2O_3 catalyzed experiments from 1-165°C

Methane samples were equilibrated from 1-165°C using γ-Al_2O_3 as a catalyst to activate methane C-H bonds[40,41]. Pellets of γ-Al_2O_3 (Alfa Aesar) were purchased and activated following a procedure modified from Robertson and co-workers[41] and based on that described by Turner and co-workers[37]. γ-Al_2O_3 pellets were added to quartz tubes (10 pellets or 0.24-0.28 g per tube) and torched under vacuum to baseline ($<10^{-3}$ torr) to drive off adsorbed air and water (10-20 min). Tubes with pellets were then heated at ~550˚C in the presence of O_2 (~100 Torr) for 5 hours and then under vacuum (while still held at 550°C) for 12-14 additional hours prior to being flame sealed by torch under vacuum in the tubes. The activated γ-Al_2O_3 pellets were stored in the sealed quartz tubes under vacuum at room temperature until used.

For a given methane equilibration experiment, ~0.5 g of activated γ-Al_2O_3 pellets (20 pellets) were added to a 20 ml borosilicate crimp top headspace vial (SUN SRi), sealed with a crimped septum stopper (blue chlorobutyl; Bellco Glass), and immediately evacuated to baseline ($<10^{-3}$ torr) through a needle attached to the vacuum line *via* an Ultra-Torr fitting (Swagelok). After removal from the vacuum line, the vial was immediately injected with ~30 ml of house methane (STP) taken from prefilled Tedlar gas bag (SKC Inc). The vial was then placed in a temperature-controlled apparatus. For the 50-165°C experiments, samples were heated using dry-block heaters with digital temperature set points (VWR); for the 25°C experiment a 5 L water bath was used with a digital temperature set point; for the 1˚C experiment a convertible refrigerator/freezer was used (572 L capacity; Kenmore).

For the 25-165°C experiments, temperature was monitored using a Type K Chromel/Alumel thermocouple. For the 1°C experiment, a USB temperature datalogger (Extech) was used. The time allowed for equilibration prior to sub-sampling was chosen to be in excess of the apparent equilibration times required to attain hydrogen isotope equilibrium between CH_4 and H_2 catalyzed by activated γ-Al_2O_3 determined by Turner and co-workers[37] using a bracketing approach[42]. We have assumed here that internal isotopic equilibrium of methane is reached over comparable timescales — we consider this a valid assumption because the equilibration of hydrogen isotopes between methane and hydrogen gas has been demonstrated to proceed at similar rates as between methane isotopologues (*cf.* ref[43]).

Methane samples (3-5 ml) were extracted from vials using gas-tight syringes (VICI) and immediately injected into a vacuum line for cryogenic purification (see below). Sampling was conducted without removing the vial from temperature control apparatus for the 25-165˚C experiments in order to avoid temperature perturbations during sampling (i.e., the catalyst remained at the reported temperature during sampling). We minimized the effect of sampling on temperature during the sampling of the refrigeration experiment (1˚C) by completing sampling within ~1-2 min of opening the refrigerator door.

2.2.2 Catalyzed experiments from 250-500°C using nickel

Equilibration experiments of methane at higher temperatures (250-500˚C) were performed using a nickel catalyst (~66% nickel on silica-alumina; Alfa Aesar) in Pyrex tube experiments following procedures described previously[5]. Briefly, nickel catalyst powder was added to Pyrex tubes and packed with glass wool (Sigma Aldrich). 5A molecular sieve (10 pellets, 1-2 mm dia. by ~5 mm in length; Alfa Aesar) was loaded on top of the glass wool. Both nickel and sieve were torched under vacuum to drive off sorbed gases (20 min) prior to quantitatively condensing methane on the sieve using liquid nitrogen and flame sealing the Pyrex tubes. Experiments were placed in the center position of a box furnace (Lindberg/Blue M; ThermoFisher Scientific) and maintained at the designated temperature (250-500˚C) for the specified duration. At the end of the experiment, samples were quenched to room temperature in <30 s using compressed air.

2.3 Methane purification and introduction to the mass spectrometer

Methane from either type of equilibration experiment (γ-Al_2O_3 or Ni) was purified on a glass vacuum line using a cryostat (Cryodyne Refrigerator System; CTI-Cryogenics, Brooks Automation, Inc.) prior to isotopic analysis following a protocol based on previous studies[5,15]. Briefly, methane is first frozen at 20K in the cryostat (10-15 min equilibration time) and any non-condensable gases present in the headspace of the line are evacuated ($\leq$ 2 min; i.e., H_2 produced during the nickel experiments). Remaining non-condensable gases trapped in the condensed methane (i.e., H_2 in the nickel experiments or trace air in the γ-Al_2O_3 experiments introduced during syringe sampling) are then removed by first bringing the cryostat to 45K, evacuating the non-condensable gases released at this temperature (0.5-2 min), and then implementing a thaw-freeze-evacuation procedure 3-5 times until the release of non-condensable gas from condensed methane is no longer detected (< 10^{-3} Torr). Finally, the methane is quantitatively distilled from the cryostat at 70K to 5A molecular sieve (10 pellets; pre-treated by torch under vacuum for 20 min) contained in Pyrex submerged in liquid nitrogen and flame-sealed and stored until analysis. Methane frozen to sieve is introduced into the inlet of the 253 Ultra for IRMS analysis using a break seal after heating the sieve at ~150˚C for 3-4 hours[5].

2.4 Mass spectrometry: 253 Ultra

In this section we describe how the isotopic measurements are made. This is done in detail because resolved $^{13}CH_3D$ and $^{12}CH_2D_2$ methane clumped-isotope measurements on the mass spectrometer used (ThermoFisher 253 Ultra) have not yet been described outside of conference proceedings[36,44]. The mass spectrometry schemes described here were originally created to measure fragment methyl groups derived from larger molecules as described by Lloyd and co-workers[45] and adopted for methane measurements. Measurements are organized into 'blocks'. At the start of a block, the sample and standard are pressure balanced. Following this, the working gas standard and sample are measured in a series of 'cycles' comprised of integrations and sub-integrations following typical sample/standard bracketing techniques for dual inlet isotope-ratio measurements. The total measurement time for δD, $\delta^{13}C$, $\Delta_{^{13}CH_3D}$, and $\Delta_{^{12}CH_2D_2}$ for a single methane sample is approximately 20-21 hours (i.e., 1 sample *per* day).

2.4.1 Measurement of $[^{12}CH_3D^+]/[^{12}CH_4^+ + {}^{12}CH_2D^+]$

The ratio of $[^{12}CH_3D^+]/[^{12}CH_4^+ + {}^{12}CH_2D^+]$ is determined to derive sample δD values. This measurement is performed in medium-resolution mode (~16 μm entrance slit) with the aperture set to HR+. The mass-16 ion beam consists of $^{12}CH_4^+ + {}^{12}CH_2D^+$ and is measured on the L1 Faraday cup using a 10^{10} Ω amplifier with a typical intensity of 2.5-2.8×10^9 counts per second (cps). The mass-17 ion beam consists of $^{12}CH_3D^+$ and is measured on the H4 Faraday cup using a 10^{12} Ω amplifier with a typical intensity of 1×10^6 cps. The mass resolving power (5,95%) is tuned to between 20-25,000. At these resolutions, the H4 cup's narrow exit slit (0.04 mm) allows $^{12}CH_3D^+$ to be resolved from other proximal mass-17 ions such as $^{13}CH_4^+$ and the $^{12}CH_5^+$ adduct (Fig. 1a). Mass-16 is measured on the flat shoulder of $^{12}CH_4^+$ where there is a contribution of the $^{12}CH_2D^+$ fragment. This is accounted for during data processing as described in Section SI.1.

Four measurement blocks consisting of 21 integrations are performed (corresponding to 10 cycles of sample/standard brackets) and begin with an automatic pressure balance. Each integration is comprised of a peak center on $^{12}CH_3D^+$ that is followed by 75 sub-integrations of 0.524 s. We peak center on every integration to ensure the measurement remains on peak due to the narrow region of peak flatness on the H4 cup (Fig. 1a). Following the four measurement blocks, the background is measured at higher mass (+0.1 Da) while gas is flowing in for the working gas and the sample. The mean background of both is removed from the measured ion beam intensities of each. The total analysis time for this measurement is approximately 2.5 hours. A diagram summarizing this measurement is provided in Fig. SI.2.

2.4.2 Measurement of $[^{13}CH_4^+]/[^{12}CH_4^+ + {}^{13}CH_3^+ + {}^{12}CH_2D^+]$ and $[^{13}CH_3D^+]/[^{12}CH_4^+ + {}^{13}CH_3^+ + {}^{12}CH_2D^+]$

The ratios of $[^{13}CH_4^+]/[^{12}CH_4^+ + {}^{13}CH_3^+ + {}^{12}CH_2D^+]$ and $[^{13}CH_3D^+]/[^{12}CH_4^+ + {}^{13}CH_3^+ + {}^{12}CH_2D^+]$ are measured together and used to determine the $\delta^{13}C$ and $\Delta_{^{13}CH_3D}$ values of sample. This measurement is performed in high-resolution mode (5 μm entrance slit) with the aperture set to standard. The mass 16 ion beam is made up of $^{12}CH_4^+ + {}^{13}CH_3^+ + {}^{12}CH_2D^+$ and is registered on the L4 Faraday cup using a 10^{10} Ω amplifier with a typical signal intensity of 1.4-1.6×10^9 cps. The mass-17 ion beam consists solely of $^{13}CH_4^+$ and is registered on the L2 Faraday cup through a 10^{12} Ω amplifier with a typical signal intensity of 2×10^7 cps. Finally, the mass-18 ion beam consists solely of $^{13}CH_3D^+$ and is registered on the H3 compact discrete dynode (CDD) secondary electron multiplier with a typical signal intensity of 8000 cps. The mass resolving power is tuned to 28-30,000 (5,95%) such that $^{13}CH_4^+$ and $^{13}CH_3D^+$ are measurable on flat shoulders (Fig. 1b and 1c). The measurement is performed in 8 blocks where each block is comprised of 21 standard/sample integrations (corresponding to 10 cycles *per* block that represent sample/standard brackets). Each integration consists of 60 discretized 1.05s sub-integrations. Measurements are centered on the flat shoulder of $^{13}CH_3D^+$. This center position is determined every two blocks (4× total) beginning with the first block. Background measurements for all beams (masses 16, 17, and 18) for the sample and then the working gas are performed at the end of every two blocks (4× total) by moving down-mass (-0.0089 Da) while gas is flowing into the source. In the case of each ion beam, the mean background of the sample and working gas is taken and then subtracted from the raw intensities of both sample and working gas for each block pair. The presence of the $^{13}CH_3^+ + {}^{12}CH_2D^+$ fragments on the mass 16 intensity are corrected for as described in Section SI.1. The

total analysis time for this measurement is approximately 5.5 hours. A diagram summarizing this measurement is provided in Fig. SI.3.

2.4.3 Measurement of $[^{12}CH_2D_2^+]/[^{12}CH_4^+ + {}^{13}CH_3^+ + {}^{12}CH_2D^+]$

The $[^{12}CH_2D_2^+]/[^{12}CH_4^+ + {}^{13}CH_3^+ + {}^{12}CH_2D^+]$ ratio is measured to determine the $\Delta_{^{12}CH_2D_2}$ value of a sample. This measurement is performed in high-resolution mode (5 μm entrance slit) with the aperture set to standard. The mass-16 ion consists of $^{12}CH_4^+ + {}^{13}CH_3^+ + {}^{12}CH_2D^+$ and is registered on the L3 Faraday cup with a 10^{10} Ω amplifier with a typical signal size of 1.4-1.8×10^9 cps. The mass-18 ion beam consists of $^{12}CH_2D_2^+$ and is registered on the H4 CDD with a typical signal size of 60-100 cps. The mass resolving power is tuned to 28-32,000, (5,95%) such that $^{12}CH_2D_2^+$ is separated from proximal mass-18 adducts ($^{13}CH_5^+$ and $^{12}CH_4D^+$; Fig. 1d).

The measurement is performed in 18 blocks where each block is comprised 21 standard/sample integrations (i.e., 10 cycles of sample/standard brackets). Each integration begins with a peak center on $^{13}CH_3D^+$ that is followed by a magnet peak hop of 0.00292 Da to the center of $^{12}CH_2D_2^+$. We then perform 60 discretized 1.05 s sub-integrations. A background measurement is taken at the end of the last block by moving up in mass (+0.1 Da) while gas is flowing. The mean background for sample and working gas is determined and then subtracted from both the sample and working gas ion-beam intensities. The total analysis time for this measurement is approximately 12-13 hours. Finally, we correct for the contributions of peak tailing of the adjacent $^{13}CH_3D^+$ and $^{13}CH_5^+$ peaks to the total background at $^{12}CH_2D_2^+$ based on the methodology originally devised and presented by Xie and co-workers[44]. These corrections are typically ~ 0.35 cps. A description of this correction is provided in detail in Section SI.2. A diagram summarizing this measurement is provided in Fig. SI.4.

2.4.4 Calculation of δD, $\delta^{13}C$, $\Delta_{^{13}CH_3D}$, and $\Delta_{^{12}CH_2D_2}$ values

The calculation of δD, $\delta^{13}C$, $\Delta_{^{13}CH_3D}$, and $\Delta_{^{12}CH_2D_2}$ values from the above ratios requires a correction be made for the $^{12}CH_2D^+$ and $^{13}CH_3^+$ fragments present in the measurements. This is done by determining a fragmentation ratio that describes the relative abundance of a fragment methyl ion *vs*. an unfragmented methane ion. The fragmentation ratio for methyl groups from methane is determined operationally during the $[^{13}CH_4^+]/[^{12}CH_4^+ + {}^{13}CH_3^+ + {}^{12}CH_2D^+]$ measurement (see Section 2.4.2) by measuring the $[^{13}CH_3^+]/[^{13}CH_4^+]$ ratio after every two blocks before the background measurements are taken (4× total). The fragmentation ratio for the 253 Ultra at UC Berkeley is ~0.8, which is the same as that measured by Stolper and co-workers[5] on the 253 Ultra prototype instrument. From the measured ion ratios above and the determined fragmentation ratio, the δD, $\delta^{13}C$, $\Delta_{^{13}CH_3D}$, and $\Delta_{^{12}CH_2D_2}$ can be determined. The equations used to do this are given in Section SI.1.

Calculation of $\Delta_{^{13}CH_3D}$ and $\Delta_{^{12}CH_2D_2}$ for a measured sample requires knowledge of the $\Delta_{^{13}CH_3D}$ and $\Delta_{^{12}CH_2D_2}$ composition of the working gas (house methane), which *a priori* is unknown. Therefore, measurements are initially placed into a 'working gas reference frame' by assuming that the compositions of the working gas correspond to $\Delta_{^{13}CH_3D}$ = 0‰ and $\Delta_{^{12}CH_2D_2}$= 0‰. Measurements reported in the 'working gas reference frame' in this study will be denoted with a subscript 'wg'

for clarity (i.e., $\Delta^{13}_{CH_3D(wg)}$, and $\Delta^{12}_{CH_2D_2(wg)}$). We emphasize that measurements reported relative to a working gas are in an arbitrary reference frame that is not rooted in thermodynamics or internationally recognized standards (which do not exist for methane clumped-isotope measurements). Such measurements can and will be converted to the 'thermodynamic' (or absolute) reference frame as covered in Section 4.1 based on our experiments and theoretical calculations.

2.5 Theoretical calculations of equilibrium methane clumping

This section briefly describes how partition function ratios (PFRs) are computed using the PIMC (e.g., refs[11,35]) and BMU[29,30] theoretical frameworks. In this study, the potential energy surface for methane, which is required for both the PIMC and BMU calculations, is taken from Lee and co-workers[34]; this potential energy surface is constructed from calculations at the CCSD(T) level of theory using cc-pVTZ and cc-pVQZ basis sets (see Lee and co-workers[34] for additional details regarding the construction of the potential energy surface). We base our PIMC and BMU theoretical calculations on the same potential energy surface for methane[34] in order to obtain a direct comparison between the two theoretical approaches for computing PFRs.[11]

2.5.1. Path Integral Monte Carlo (PIMC) calculations

The Path Integral Monte Carlo (PIMC) technique employs the imaginary-time path integral formalism[46] to map the quantum mechanical partition function (PF) onto a classical PF[47],

$$Q(N,\beta) = \lim_{P\to\infty} \frac{1}{\sigma}\prod_{i=1}^{N}\left(\frac{m_i P}{2\pi\beta\hbar^2}\right)^{\frac{3P}{2}} \int\prod_{j=1}^{N}\prod_{k=1}^{P} d\boldsymbol{r}_j^{(k)} e^{-\beta_P U_P\left(\left\{\boldsymbol{r}_j^{(k)}\right\}\right)}, \quad (7)$$

such that the quantum Boltzmann statistics of the *N*-particle system is obtained from the classical statistics of a ring-polymer with P beads at inverse temperature $\beta_P=\beta/P$ that interact *via* an effective potential,

$$U_P\left(\left\{\boldsymbol{r}_j^{(k)}\right\}\right) = \sum_{j=1}^{N}\sum_{k=1}^{P}\frac{m_j\omega_P^2}{2}\left(\boldsymbol{r}_j^{(k)} - \boldsymbol{r}_j^{(k-1)}\right)^2 + \sum_{k=1}^{P} U\left(\boldsymbol{r}_1^{(k)}, ..., \boldsymbol{r}_N^{(k)}\right). \quad (8)$$

Here, $\boldsymbol{r}_j^{(k)}$ indicates the position of the jth atom in the kth ring-polymer bead, $\omega_P = 1/(\beta_P\hbar)$ is the intra-bead vibrational frequency, $\boldsymbol{r}_j^{(0)} = \boldsymbol{r}_j^{(P)}$, and $U(\boldsymbol{r}_1, ..., \boldsymbol{r}_N)$ is the Born–Oppenheimer potential energy surface for the molecular system. Note that the indistinguishability of identical nuclei in the PI calculations in Eq. 7 is treated using the classical rotational symmetry number, σ, since effects related to nuclear exchange statistics are expected to be negligible for the temperatures and isotope-exchange reactions considered in this study.

The methodology for computing PFRs and equilibrium constants in this study follows that employed by Webb and co-workers[35] and is only briefly reviewed here. In short, a direct scaled-coordinate estimator[48] is used to calculate the PFRs. Heavy isotopologue configurations are sampled with PIMC in Cartesian coordinates with an explicit staging transformation[49]. The staging length, *j*, is set such that 38−42% of all proposed staging moves are accepted. Prior to any data collection, each sampling trajectory is equilibrated for 10^5 MC steps, with *P*/*j* staging moves (rounded up to the nearest integer) attempted per MC step. Thereafter, ring-polymer configurations are sampled every 10 MC steps. The total number of MC moves for each PFR calculation is 2×10^8 (10^9 for select *T* values: 1.2, 50.5, 75.7, 127.8, and 165.4˚C). There are two primary sources of error in the PIMC calculations, aside from any errors due to the potential energy surface. The first

is systematic error related to convergence of the PFs (or derived quantities) with the number of beads; this error vanishes in the limit of infinite beads as expressed in Eq. 7. The second is statistical error related to sampling of the direct scaled-coordinate estimator for the PFRs; this error vanishes in the limit of infinite sampling. In this study, the number of beads employed in the PIMC calculations is determined based on explicit convergence tests for the individual PFRs (see Fig. SI.5) and summarized in Table SI.1. All errors reported for the PIMC calculations reflect standard errors related to statistical uncertainty with the Monte Carlo sampling method.

2.5.2 Bigeleisen and Mayer/Urey model calculations

The partition function ratio of an isotopologue pair based on the Bigeleisen and Mayer/Urey (BMU) model[29,30] is given by[11,35]:

$$\mathrm{PFR_{BMU}} = \frac{\mathrm{Q}^*}{\mathrm{Q}} = \frac{\sigma}{\sigma^*} e^{-(E_0^* - E_0)/k_\mathrm{B}T} \prod_{i=1}^{N} \left(\frac{m_i^*}{m_i}\right)^{\frac{3}{2}} \prod_{j=1}^{a} \frac{\omega_j^* \left(1 - e^{-\hbar\omega_j/k_\mathrm{B}T}\right)}{\omega_j \left(1 - e^{-\hbar\omega_j^*/k_\mathrm{B}T}\right)}, \quad (9)$$

where σ are rotational symmetry numbers, E_0 is the zero-point energy, m_i is the mass of the *i*th atom in a molecule of N atoms, ω_j is the harmonic frequency (given as wave number) of the *j*th normal mode, a is the total number of vibrational modes ($a = 3N - 5$ for linear molecules, $a = 3N - 6$ for non-linear molecules), and * indicates the isotopically-substituted molecule. The BMU model is arranged to compute PFRs in terms of substituted isotopologues (i.e., $^{12}CH_3D$, $^{13}CH_4$, $^{13}CH_3D$, $^{12}CH_2D_2$) relative to the unsubstituted isotopologue ($^{12}CH_4$). In this study, we will diverge from this convention in reporting PFRs (after ref[11]) and will instead specify the isotopologues comprising a PFR.

The so-called Reduced Partition Function Ratio (RPFR) that is commonly reported in the stable isotope geochemistry literature (e.g., refs[9,10,31–33,50]) was first recommended by the original authors of the BMU model for simplicity[29,30] and is defined by convention as the above (Eq. 9) but is normalized for the mass terms[50] and the rotational symmetry numbers. The reasons for these normalizations comes from the traditional application of the BMU model to problems of single isotope-exchange reactions among molecules and the observation that the mass terms always cancel in the computation of fractionation factors and/or isotope exchange equilibrium constants, and that the rotational symmetry numbers are not responsible for relative isotopic differences between different phases or species[29]. We compute and discuss PFRs rather than RPFRs in this work. We provide computations of RPFRs for both PIMC and BMU calculations in the Supplementary Information (see Table SI.5). We additionally provide harmonic vibrational frequencies for methane isotopologues derived from the potential energy surface of methane of Lee and co-workers[34] in Table SI.6 that were utilized for our BMU calculations.

3. Results

3.1 Accuracy and Precision

In order to determine both our external precision as well as our accuracy, three gas standards with different bulk and clumped isotopic compositions were prepared and measured in multiple analytical sessions. The standards 'PlusD' and 'PlusD-200' were prepared to have higher δD values relative to the working gas (+88‰ and +208‰, respectively) and the 'Plus^{13}C' standard was prepared to have a higher $\delta^{13}C$ value relative to the working gas (+34‰). They were replicated

9, 8, and 4 times, respectively, over different analytical sessions. 8 distinct analytical sessions are represented in our dataset. All individual replicate measurements are provided in Table SI.2. A summary table of the average measured values along with external precisions is given in Table 1.

Based on the reproducibility of these in-house standards, we estimate that our ±1σ external precision for each measured isotopic parameter is: δD = ±0.15‰, $\delta^{13}C$ = ±0.02‰, $\Delta_{^{13}CH_3D}$ = ±0.33‰, and $\Delta_{^{12}CH_2D_2}$ = ±1.35‰. These are similar to the measured internal precisions: δD = ±0.12‰, $\delta^{13}C$ = ±0.01‰, $\Delta_{^{13}CH_3D}$= ±0.25‰, $\Delta_{^{12}CH_2D_2}$= ±1.35‰ (±1 s.e.).

In order to place our δD and $\delta^{13}C$ measurements on the VSMOW and VPDB reference scales and establish the accuracy of our measurements, the δD and $\delta^{13}C$ values of the house methane ('working gas') and in-house reference standards were measured at the Stable Isotope Facility of UC Davis following methods described in ref[39]. At this lab, methane stable-isotope measurements are anchored to international methane standards with known δD and $\delta^{13}C$ values. At UC Davis, our reference gas was triplicated for both δD and $\delta^{13}C$ while the other standards were duplicated for these parameters. The δD and $\delta^{13}C$ values of these in-house standards as determined at UC Davis relative to the VSMOW and VPDB scales are presented in Table 1. The working gas was determined to have a δD_{VSMOW} = -159.3‰ (± 2.4‰, ±1σ; ± 1.4‰, ±1 s.e.) and $\delta^{13}C_{VPDB}$ = -38.37‰ (± 0.04‰, ±1σ; ±0.02, ±1 s.e.). We assign these values to the UC Berkeley working gas. With this assignment, we can directly compare determinations of δD and $\delta^{13}C$ between samples (PlusD, PlusD-200, and Plus^{13}C) measured on the 253 Ultra at UC Berkeley and measured using conventional pyrolysis and combustion techniques at UC Davis (Table 1). The values of δD_{VSMOW} as measured on the 253 Ultra are within ≤ 4.4‰ of the conventional analyses (note: typical ±1σ external precision for δD-CH_4 at UC Davis is ±4‰[39]). A least squares linear regression of δD_{VSMOW} (conventional-UC Davis) *vs.* δD_{VSMOW} (253 Ultra-UC Berkeley) yields a slope of 1.01 ± 0.02 (1 s.e.). The 253 Ultra measurements of $\delta^{13}C_{VPDB}$ are within ≤ 0.56‰ of the conventional measurements (note: typical ± 1σ external precision for $\delta^{13}C$-CH_4 at UC Davis is ±0.2‰[39]). The distribution in values of $\delta^{13}C_{VPDB}$ for the in-house standards is insufficient to perform a meaningful regression for additional comparison (i.e., only one of the three standards differs greatly in $\delta^{13}C_{VPDB}$). Based on these comparisons, we consider our measurements of δD and $\delta^{13}C$ values using the 253 Ultra to be accurate.

We test an aspect of our $\Delta_{^{13}CH_3D}$ or $\Delta_{^{12}CH_2D_2}$ accuracy as follows. Correctly measured $\Delta_{^{13}CH_3D}$ or $\Delta_{^{12}CH_2D_2}$ for samples isotopically equilibrated at the same temperature should be constant and should not depend on δD or $\delta^{13}C$ values. To demonstrate this, we follow the approach outlined previously[5] (and based on approaches developed for CO_2 clumped isotope analyses; e.g., ref[51]) in which samples with varying bulk isotopic compositions are equilibrated at the same temperature. Specifically, samples of the house methane, PlusD, PlusD-200, and Plus^{13}C in-house standards were equilibrated at 500°C. We use δD values to test for this as they vary the most (208‰) for the standards as compared to the $\delta^{13}C$ variation (38.4‰). The results of these experiments are included in Table SI.3 and are plotted in Fig. 2.

Over a δD range of ~204‰, the slope of $\Delta_{^{13}CH_3D}$ *vs.* δD is 0.0013 ± 0.0010 (1 s.e.) and $\Delta_{^{12}CH_2D_2}$ *vs.* δD is -0.010 ± 0.010 (1 s.e.). As these slopes are statistically indistinguishable from 0 at the 2 s.e.

level, we conclude our measurements are relatively precise over ~200‰ δD ranges with no compositional dependence.

3.2 Equilibrated Gas Experiments

The average $\Delta^{13}_{CH_3D}$ and $\Delta^{12}_{CH_2D_2}$ values of the equilibrated gas experiments from 1-500°C in the working gas reference frame (i.e., where 0‰ is the Δ value of the working gas, and denoted with subscript 'wg') are presented in Table 2. Individual measurements of sample δD, $\delta^{13}C$, $\Delta^{13}_{CH_3D(wg)}$, and $\Delta^{12}_{CH_2D_2(wg)}$ values are given in Table SI.3. All experiments except those at 500°C discussed above and at 250°C were performed using the house methane ('working gas'). For the 250°C experiments, measured $\Delta^{13}_{CH_3D}$ and $\Delta^{12}_{CH_2D_2}$ using the house methane ('working gas') as the starting gas yielded values within ±1 s.e. (note: this is internal precision) of unheated working gas ($\Delta^{13}_{CH_3D(wg)}$ = -0.22 ± 0.25‰, $\Delta^{12}_{CH_2D_2(wg)}$= 1.4 ± 1.4‰, ±1 s.e.; Table SI.3). To verify that isotopic equilibrium was indeed reached at 250°C, we performed two additional experiments using a starting methane with elevated $\Delta^{12}_{CH_2D_2}$ value relative to the working gas ($\Delta^{12}_{CH_2D_2(wg)}$= 872.7 ± 1.9‰, ±1 s.e., internal precision) but otherwise similar δD, $\delta^{13}C$, and $\Delta^{13}_{CH_3D}$ compositions *vs.* the working gas ('Plus$^{12}CH_2D_2$' in Table SI.2). These experiments yielded final $\Delta^{13}_{CH_3D(wg)}$and $\Delta^{12}_{CH_2D_2(wg)}$ values within ±2 s.e. of the value obtained for the house methane experiment and thus show the nickel catalyst is sufficiently active at 250˚C to equilibrate clumped methane compositions over the timescales used (≤184 hours; Table SI.3).

All other experiments were performed with the house methane at a given temperature and were replicated at least twice and for different time durations (Tables 2 and SI.3). Experiments performed at the same temperature but for different durations do not exhibit time dependence in values of $\Delta^{13}_{CH_3D}$ and $\Delta^{12}_{CH_2D_2}$ within ±1 s.e. of the measurements (internal precision), which is evidence that internal isotopic equilibrium was reached. House methane allowed to react in the presence of the nickel catalyst (250-500˚C) exhibits bulk δD and $\delta^{13}C$ compositions that are comparable to the starting gas (i.e., within ≤ 8‰ for δD and ≤1.3‰ for $\delta^{13}C$). This is also true for the γ-Al_2O_3 experiments (1-165.4˚C) in which changes in δD are within ≤ 5‰ and changes in $\delta^{13}C$ are within ≤0.5‰; Table SI.3). The external precision of $\Delta^{13}_{CH_3D}$ and $\Delta^{12}_{CH_2D_2}$ as estimated solely from the experimental replicates at a given temperature is ±0.20‰ for $\Delta^{13}_{CH_3D}$ and ±1.78‰ for $\Delta^{12}_{CH_2D_2}$ (1σ; Table SI.3), which are similar to internal precisions and the external precisions as estimated from the long-term reproducibility of in house reference standards (±0.33‰ and ±1.35‰, respectively, ±1σ; Table 1). The total range in mean clumped compositions measured from experiments conducted over 1-500˚C is 6.3‰ for $\Delta^{13}_{CH_3D}$ and 23.6‰ for $\Delta^{12}_{CH_2D_2}$ (Table 2). For reference, previous calibrations of these values ranged from 1.0-2.2‰ for $\Delta^{13}_{CH_3D}$[5–7,14,38] and 2.2‰ for $\Delta^{12}_{CH_2D_2}$[7] (see Sections 1.2 and 1.3).

Finally, the 500˚C experiments performed with the methane of varying δD (house gas, PlusD, and PlusD-200) comprise a bracketing experiment with respect to $\Delta^{13}_{CH_3D}$ (Fig. 2a) where final values determined after heating were approached from both higher and lower starting $\Delta^{13}_{CH_3D}$ values. This is further supporting evidence for achieving equilibrium at 500˚C.

3.3 PIMC and BMU Calculations

Results of the PIMC calculations are presented in Table 3 and comparable calculations using the BMU model[29,30] are presented in Table 4. As discussed, both sets of calculations utilize the same electronic potential energy surface for methane[34], which is constructed at the CCSD(T) level of theory (see Methods Section 2.5 for more details). Values of $1000 \times \ln(K_{^{13}CH_3D})$ and $1000 \times \ln\left(\frac{8}{3}K_{^{12}CH_2D_2}\right)$ using the PIMC methods have been computed over a temperature range of -3 to 527˚C (270-800 K). The errors (±1 s.e.) on individual PIMC computations are ≤0.03‰ for $1000 \times \ln(K_{^{13}CH_3D})$ and ≤0.33‰ for $1000 \times \ln\left(\frac{8}{3}K_{^{12}CH_2D_2}\right)$.

Polynomial fits to $1000 \times \ln(K_{^{13}CH_3D})$ and $1000 \times \ln\left(\frac{8}{3}K_{^{12}CH_2D_2}\right)$ values as a function of T^{-1} (6th or 7th order, respectively, with both fits forced through an intercept of 0‰ at infinite temperature) have been applied to the PIMC results to allow interpolation between computed temperatures (-3 to 527˚C) and extrapolation above the highest computed temperature:

$$\Delta_{^{13}CH_3D} \cong 1000 \times \ln(K_{^{13}CH_3D}) = \frac{1.47348 \times 10^{19}}{T^7} - \frac{2.08648 \times 10^{17}}{T^6} + \frac{1.19810 \times 10^{15}}{T^5} - \frac{3.54757 \times 10^{12}}{T^4} + \frac{5.54476 \times 10^{9}}{T^3} - \frac{3.49294 \times 10^{6}}{T^2} + \frac{8.89370 \times 10^{2}}{T} \quad (10)$$

$$\Delta_{^{12}CH_2D_2} \cong 1000 \times \ln\left(\frac{8}{3}K_{^{12}CH_2D_2}\right) = -\frac{9.67634 \times 10^{15}}{T^6} + \frac{1.71917 \times 10^{14}}{T^5} - \frac{1.24819 \times 10^{12}}{T^4} + \frac{4.30283 \times 10^{9}}{T^3} - \frac{4.48660 \times 10^{6}}{T^2} + \frac{1.86258 \times 10^{3}}{T} \quad (11)$$

Values computed from these equations are strictly valid over 270-800 K but are also likely valid > 800 K due to the requirement that these values (as defined) must approach 0‰ at the high-temperature-limit. Note that the range in values of $1000 \times \ln(K_{^{13}CH_3D})$ and $1000 \times \ln\left(\frac{8}{3}K_{^{12}CH_2D_2}\right)$ extrapolated above 800 K to the high temperature limit are ≤ 0.75‰ and ≤ 1.3‰, respectively.

Computed values from the polynomial fits are shown Fig. 3 along with the residuals. The computed ±1σ of the residuals are ±0.02‰ and ±0.14‰ for the $1000 \times \ln(K_{^{13}CH_3D})$ and $1000 \times \ln\left(\frac{8}{3}K_{^{12}CH_2D_2}\right)$ polynomial fits, respectively, which are comparable to the stated precision of the calculations at any given temperature (see Table 3 and Fig. 3).

Computations of equilibrium constants ($K_{^{13}CH_3D}$ and $K_{^{12}CH_2D_2}$) and derived equilibrium clumped compositions $\Delta_{^{13}CH_3D}$ given as $1000 \times \ln(K_{^{13}CH_3D})$ and $\Delta_{^{12}CH_2D_2}$ given as $1000 \times \ln\left(\frac{8}{3}K_{^{12}CH_2D_2}\right)$ using Eq. 5 and 6 are comparable between the PIMC and BMU approaches (Tables 3 and 4). For example, values of $1000 \times \ln(K_{^{13}CH_3D})$ computed using the BMU model are within ≤ 0.10‰ of the PIMC values over all computed temperatures (-3-527°C). Similarly, values of $1000 \times \ln\left(\frac{8}{3}K_{^{12}CH_2D_2}\right)$ computed using the BMU model are within ≤ 0.37‰ of the PIMC values.

Despite this agreement, the BMU-based PFRs, which are used to calculate the BMU-based $1000 \times \ln(K_{^{13}CH_3D})$ and $1000 \times \ln\left(\frac{8}{3}K_{^{12}CH_2D_2}\right)$ values, are systematically higher than the PIMC PFRs. Table SI.4 contains computations of the differences between the two approaches in δ-notation: $\delta PFR_{(BMU\text{-}PIMC)} = 1000 \times (PFR_{BMU}/PFR_{PIMC} - 1)$, and $\delta K_{(BMU\text{-}PIMC)} = 1000 \times (K_{BMU}/K_{PIMC} - 1)$

(reported in units of ‰). The $\delta PFR_{(BMU-PIMC)}$ are as high as 5-6‰ for the $^{13}CH_4/^{12}CH_4$ and $^{13}CH_3D/^{12}CH_3D$ PFRs and 29-95‰ for the $^{12}CH_3D/^{12}CH_4$ and $^{12}CH_2D_2/^{12}CH_3D$ PFRs over the computed temperature range. We note that comparable computations of RPFRs for $^{12}CH_3D/^{12}CH_4$ and $^{13}CH_4/^{12}CH_4$ (Table SI.5) yield the same relative differences between PIMC and BMU approaches (in terms of analogous $\delta RPFR_{(BMU-PIMC)}$ comparisons) as is expected given the cancelation of rotational symmetry numbers and the mass terms in values of $\delta PFR_{(BMU-PIMC)}$ that are normalized out in the RPFR calculations by convention.

4. Discussion

4.1 Experiment vs. Theory (PIMC): Working Gas Calibration

Fig. 4 compares measured *vs.* PIMC theoretical clumped isotope compositions computed at the experimental temperatures. For this comparison, we compare experimentally measured values as $1000\times\ln(\Delta_{(wg)}/1000+1)$ values (where the $\Delta_{(wg)}$ value represents $\Delta_{^{13}CH_3D(wg)}$ or $\Delta_{^{12}CH_2D_2(wg)}$ values as measured and reported in Tables 2 and SI.3) *vs.* computed values of $1000\times\ln(K_{^{13}CH_3D})$ and $1000\times\ln\left(\frac{8}{3}K_{^{12}CH_2D_2}\right)$. This comparison limits approximations associated with measured *vs.* theoretical clumped-isotope compositions (see ref[25] and our Eq. 5 and 6)‡.

A least squares linear regression through each measured *vs.* theory (PIMC) dataset yields a slope of 1.02 ± 0.04 for the $\Delta_{^{13}CH_3D}$-based comparison and 0.98± 0.05 for the $\Delta_{^{12}CH_2D_2}$-based comparison (±1 s.e.). Thus, both slopes are within 1 s.e. error of 1 over a temperature range of 1-500°C. Given this 1:1 agreement between experiment and theory, lines with slopes ≡ 1 are used to infer the intercept in each plot to obtain estimates of the working gas composition. These yield $\Delta_{^{13}CH_3D}$ = 2.59 ± 0.14‰ and $\Delta_{^{12}CH_2D_2}$ = 5.86 ± 0.60‰ (±1 s.e.)§. We emphasize that these values for the working gas are in the thermodynamic reference frame where Δ = 0‰ occurs at infinite temperature.

Table 2 contains the average $\Delta_{^{13}CH_3D}$ and $\Delta_{^{12}CH_2D_2}$ values of our experimental gases equilibrated at different temperatures (individual experimental data in Table SI.3) converted to the thermodynamic reference frame using the $\Delta_{^{13}CH_3D}$ and $\Delta_{^{12}CH_2D_2}$ values determined for the working gas. These values are further converted to $1000\times\ln(\Delta/1000+1)$ values and compared to PIMC calculations of $1000\times\ln(K_{^{13}CH_3D})$ and $1000\times\ln\left(\frac{8}{3}K_{^{12}CH_2D_2}\right)$ in Table 5 and in Fig. 5. As expected from the 1:1 agreement in the temperature dependence indicated in Fig. 4, the experimental data match the predicted temperature dependence from the PIMC calculations over 1-500˚C. The computed ±1σ of the residuals are ±0.22‰ and ±1.17‰ for the $^{13}CH_3D$ and $^{12}CH_2D_2$ comparisons, respectively (Table 5). These are similar to the external precision estimated solely from the

‡ Note: The $1000\times(R/R^*-1) \cong 1000\times\ln(R/R^*)$ approximation holds for the measured compositional range of $\Delta_{^{13}CH_3D(wg)}$ and $\Delta_{^{12}CH_2D_2(wg)}$ (i.e., differences between the two notations are ca. ≥10× smaller than the precision of the measurements) and our choice makes no significant difference on the results or interpretations of our calibration. Nevertheless the $1000\times\ln(R/R^*)$ *vs.* $1000\times\ln(K_{^{13}CH_3D})$ or $1000\times\ln\left(\frac{8}{3}K_{^{12}CH_2D_2}\right)$ comparisons of measurements *vs.* theory for isotopically equilibrated systems is more accurate.

§Note: These values are in the $\Delta = 1000\times(R/R^*-1)$ notation.

experimental replicates at a given temperature (±0.20‰ for $\Delta^{13}CH_3D$ and ±1.78‰ for $\Delta^{12}CH_2D_2$, 1σ; Section 3.2). Finally, we provide a comparison of previously measured $\Delta^{13}CH_3D$ and $\Delta^{12}CH_2D_2$ values for samples experimentally equilibrated at known temperatures (refs[6,7,14,38]) *vs.* our data and PIMC theoretical curves in Fig. SI.6. The comparison shown in Fig. SI.6 of experimentally determined equilibrium $\Delta^{13}CH_3D$ and $\Delta^{12}CH_2D_2$ values as a function of temperature also shows agreement with the theoretical equilibrium temperature dependence of methane clumping presented here (i.e., determinations from other labs[6,7,14,38] are within ~0.2‰ and ~0.5‰ for $\Delta^{13}CH_3D$ and $\Delta^{12}CH_2D_2$, respectively, over the determined temperature ranges).

This work yields the important and satisfying result that theoretically calculated $\Delta^{13}CH_3D$ and $\Delta^{12}CH_2D_2$ values using the most rigorous theoretical approach available (PIMC) are in 1:1 agreement (at the ±1 s.e. level) with experimental determinations of equilibrium $\Delta^{13}CH_3D$ and $\Delta^{12}CH_2D_2$. This provides confidence in both the theory, experiments, and measurement techniques over essentially the full range of formation temperatures of microbial and thermogenic gases on earth. Furthermore, agreement in $\Delta^{13}CH_3D$ and $\Delta^{12}CH_2D_2$ values of experimentally equilibrated samples between various laboratories (Fig. SI.6) despite different measurement techniques, working gases, and theoretical calculations utilized for calibrations is encouraging and indicates that measurements between laboratories can likely be directly compared.

Finally, the working gas clumped compositions converted appropriately to $1000\times\ln(\Delta/1000+1)$ values yield apparent methane-clumped isotope temperatures of 196 ± 13˚C for $\Delta^{13}CH_3D$ and 204 ± 17˚C for $\Delta^{12}CH_2D_2$ (±1 s.e.) using the polynomial fits to the PIMC calculations (Eq. 10 and 11). Based on the δD_{VSMOW} (-159.3 ± 2.4‰, ±1σ) and $\delta^{13}C_{VPDB}$ (-38.37 ± 0.04‰, ±1σ) values of the working gas, the cylinder gas is likely thermogenic in origin[1,2]. Such temperatures are reasonable potential gas formation temperatures[28] and are consistent with the common observation that apparent methane clumped isotope temperatures of thermogenic methane are compatible with expectations of thermogenic gas formation temperatures[7,12,14,15,20].

The $\Delta^{13}CH_3D$- and $\Delta^{12}CH_2D_2$-based temperatures are within ±1 s.e. of each other. Such agreement has been previously seen both in assumed thermogenic gases from commercially purchased cylinders[24] as well as thermogenic gases from natural gas deposits[7,12]. Such agreement has been taken as additional evidence that thermogenic gases may form in clumped-isotope equilibrium and that $\Delta^{13}CH_3D$ and $\Delta^{12}CH_2D_2$ may represent formation temperatures of thermogenic gases (or at least re-equilibration temperatures).

Given the agreement in clumped-based temperatures of our working gas inferred for both $\Delta^{13}CH_3D$ and $\Delta^{12}CH_2D_2$, we could choose to force our working gas to have a $\Delta^{12}CH_2D_2$ composition that corresponds to the temperature derived from the $\Delta^{13}CH_3D$ calibration (~196˚C) given that the $\Delta^{13}CH_3D$ measurements are more precise. This exercise would yield a $\Delta^{12}CH_2D_2$ value of ~6.17‰ for our working gas derived from Eq. 11, which is about 0.31‰ higher than, but within 1 s.e. of what we directly infer from our calibration (5.86 ± 0.60‰, 1 s.e.). This may mean that our future measurements of $\Delta^{12}CH_2D_2$ could be biased to ca. 0.3‰ lower values based on our calibration if our working gas is actually in internal isotopic equilibrium (which is not known). Given our current

typical external precision (1.35‰, ±1σ) we do not expect that any such bias would change any interpretations of environmental or experimental samples.

4.2 PIMC methods vs. traditional BMU models

PIMC calculations provide a way to compute stable isotope fractionation factors independent of the traditionally implemented BMU model. As the PIMC calculations inherently include a fully anharmonic and quantum mechanical description of the partition function ratios, they are considered to be more rigorous than BMU calculations such that comparison of BMU and PIMC calculations can be used to identify errors in BMU calculations[11,35]. In the current study, all BMU-PFRs exhibit significant departures from the PIMC-PFRs: up to 5-6‰ for $^{13}CH_4/^{12}CH_4$ and $^{13}CH_3D/^{12}CH_3D$ PFRs and 95-29‰ for the $^{12}CH_3D/^{12}CH_4$ and $^{12}CH_2D_2/^{12}CH_3D$ PFRs over the computed temperature range (-3 to 527˚C). As noted earlier, the same relative differences are preserved when $^{13}CH_4/^{12}CH_4$ and $^{12}CH_3D/^{12}CH_4$ PFRs are transformed into comparable RPFRs that are more commonly reported in the stable isotope literature (e.g., refs[9,10,31–33]; Tables SI.4 and SI.5). Given that both BMU and PIMC computations were performed using the same electronic potential energy surface for methane computed using high level coupled cluster theory[34], these are true differences between the BMU and PIMC theoretical treatments as opposed to differences due to different potential energy surfaces. The $^{12}CH_3D/^{12}CH_4$ PFRs calculated using the BMU *vs.* PIMC approach exhibit 5-20x larger relative differences than $^{13}CH_4/^{12}CH_4$ PFRs. We propose that the larger discrepancy present for D/H exchange is likely due to the long-recognized inadequacies in the simplified treatments of partition functions in the BMU model to account properly for D/H exchange (e.g., harmonic vibrational PF and classical rotational PF; e.g., refs[29,30,32,33]). The PIMC calculations inherently account for vibrational anharmonicity and quantize the rotational motions, and therefore avoid these well-understood approximations inherent to the BMU approach[29,30,32,33].

Additional insight into the problem may be given by comparisons between the calculations of the present study (BMU *vs.* PIMC) and previous BMU calculations of methane performed without and with *ex post facto* corrections reported by Liu and Liu[9] following earlier correction schemes[32,33]. We first note that such a comparison is ultimately inexact because their[9] calculations are based on an electronic potential energy surface for methane computed at the MP2 level of theory (aug-cc-pVTZ basis set) rather than the more accurate couple cluster theories of the present study (CCSD(T), cc-pVTZ and cc-pVQZ basis sets; see ref[34] for more detail). The corrections implemented by Liu and Liu[9] include those for vibrational anharmonicity (e.g., anharmonic contributions to the zero point energy and anharmonic contributions to vibrational excited states) and quantum corrections to rotational motions among others[9,33], which are applied *ex post facto* to harmonically computed RPFRs[9,33]. The relative difference between uncorrected and corrected $^{12}CH_3D/^{12}CH_4$ RPFRs (104 to 34‰ over 0 to 500˚C, respectively) and $^{13}CH_4/^{12}CH_4$ RPFRs (5.4 to 1.9‰ over 0 to 500˚C, respectively) using the BMU model by Liu and Liu[9] is of similar magnitude and sign in both cases to what we observe between BMU and PIMC calculations in this study (93 to 30‰ and 5.4-1.8‰ for $^{12}CH_3D/^{12}CH_4$ and $^{13}CH_4/^{12}CH_4$, respectively, over the comparable *T* range of 1.2-501.9˚C; Tables SI.4 and SI.5). In the case of both the $^{12}CH_3D/^{12}CH_4$ and $^{13}CH_4/^{12}CH_4$ RPFRs, the total correction given by Liu and Liu[9] (multiplicative factors of ~0.906 to ~0.968 for $^{12}CH_3D/^{12}CH_4$ from 0˚C to 500˚C, and similarly 0.995 to 0.998 for $^{13}CH_4/^{12}CH_4$) is almost entirely driven by the correction for the anharmonic contributions to the zero point energy (see their[9] Table 3). This may suggest that the harmonic treatment of the

vibrational partition function may be the source of much of the error in BMU-based computations for methane.

Regardless of the precise source of the errors in the BMU model, the contrastingly small (≤0.1-0.4‰) relative differences in the computed equilibrium constants and related Δ values describing equilibrium clumping in methane from BMU-based PFRs arises from a cancelation of errors in component PFRs as observed by Webb and Miller[11]. One likely reason for this precise cancelation of errors may be due to inherent symmetry preserved in these isotopic clumping reactions. In particular, any errors present in the $^{13}CH_4/^{12}CH_4$ PFR are expected to be similar in nature and magnitude to those present in the $^{13}CH_3D/^{12}CH_3D$ PFR, since the PFRs reflect the same type of isotopic substitution. The same cannot be said for some exchange reactions involving isotopomers (e.g., $^{14}N^{15}N^{16}O \rightleftharpoons {}^{15}N^{14}N^{16}O$) for which BMU calculations have been shown to only benefit from a partial cancelation of errors[11]. Although the PFR errors appear significant when compared on a per mil scale, such errors only amount to relative free energy differences of approximately 10^{-3} and 2×10^{-2} kcal/mol for the $^{13}C/^{12}C$-related and D/H-related PFRs, respectively.

As a final note, previous theoretical calculations of clumped methane equilibrium constants based on the BMU model that have served as the basis of previous 'heated gas calibrations' (e.g., refs[6,7,14]) or that have otherwise been reported[8–10,31] compare well to the values of the present study that are based on PIMC approaches due to this cancelation of errors in individual BMU partition function ratios. For example, theoretical calculations of $\Delta_{^{13}CH_3D}$values as given by $1000 \times \ln\left(K_{^{13}CH_3D}\right)$ from refs[6–10] are all within ≤0.2‰ of the PIMC calculations presented here (Eq. 10; $T \geq 0^{\circ}C$). Similarly, the $\Delta_{^{12}CH_2D_2}$ values as given by $1000 \times \ln\left(\frac{8}{3}K_{^{12}CH_2D_2}\right)$ based on the calculations of Young and co-workers[7] and Piasecki and co-workers[10] are within ≤ 0.35‰ and ≤ 0.1‰, respectively, of the PIMC calculations presented here (Eq. 11; $T \geq 0^{\circ}C$). It is encouraging that different theoretical treatments arrive at similar values for clumped methane equilibrium constants upon which all previous clumped methane isotope measurements are anchored[5–7,14]. However, the reliance upon error cancelation to achieve relative accuracy will have to be carefully considered when applying BMU treatments of partition function ratios to problems of calculating fractionation factors between methane and other compounds (e.g., equilibrium D/H partitioning in CH_4 *vs.* H_2)[37] given that error cancellation may not be as precise when comparing different molecular substances.

5. Conclusions

We summarize the conclusions of this study as follows:

1. We presented a new mass-spectrometric technique to measure methane δD, $\delta^{13}C$, $\Delta_{^{13}CH_3D}$, and $\Delta_{^{12}CH_2D_2}$with external precisions (±1σ) of 0.15, 0.02, 0.33, and 1.35‰, respectively. Accuracy for δD and $\delta^{13}C$ were determined through measurement of in-house standards with independently measured values. Accuracy for $\Delta_{^{13}CH_3D}$ and $\Delta_{^{12}CH_2D_2}$was determined by demonstrating that gases with different δD values (208‰ range) equilibrated at 500°C show no statistically resolvable (±2 s.e.) dependence of Δ values on bulk δD values.

2. We presented a new experimental and theoretical working gas calibration method utilizing both γ-Al_2O_3 an Ni catalysts to allow for both $^{13}CH_3D$ and $^{12}CH_2D_2$ equilibrations

from 1-500°C, covering the range of expected thermogenic and microbial gas formation temperatures on earth.

3. We presented new path integral calculations (PIMC) of equilibrium clumping in methane over the same temperature range for both $^{13}CH_3D$ and $^{12}CH_2D_2$.

4. We observed 1:1 agreement (within ± 1 s.e.) between measured differences in $^{13}CH_3D$ and $^{12}CH_2D_2$ abundances for samples equilibrated from 1-500°C *vs.* those theoretically computed (PIMC) over the same temperature range.

5. The PIMC calculations can be used to gain insight into the potential sources of error in traditional approaches (BMU model), which appear to arise predominantly from the simplified treatment of partition functions in the BMU model (i.e., harmonic vibrational PF and classical rotational PF). Such insights are important for considering theoretical calculations of hydrogen isotope fractionation factors for different molecules (e.g., CH_4 *vs.* H_2) based on the BMU model.

6. Acknowledgements

DLE and DAS acknowledge research support from the Laboratory Directed Research and Development Program of Lawrence Berkeley National Laboratory under U.S. Department of Energy Contract No. DE-AC02-05CH11231. DAS acknowledges support for ACT from the National Science Foundation under Grant No. EAR-1911296 and the Donors of the American Chemical Society Petroleum Research Fund. MKL acknowledges support from the Agouron Institute. TFM acknowledges support from the National Science Foundation under Grant No. CHE-1611581. The 253 Ultra Mass Spectrometer was funded by the Heising-Simons Foundation and the University of California, Berkeley. Mark Conrad and Markus Bill (LBNL) are thanked for helpful conversations regarding standardization. Xuecheng Tao (Caltech) is thanked for helpful conversations regarding PIMC calculations.

7. Supporting Information: Section SI.1: Description of the fragment-correction scheme to determine δD, $\delta^{13}C$, $\Delta_{^{13}CH_3D,}$ and $\Delta_{^{12}CH_2D_2}$ from measured isotopologue ratios that include fragments; Section SI.2: Description of peak tailing corrections on $^{12}CH_2D_2^+$ intensity using water peak scans (including Fig. SI.1 illustrating the water peak exercise); Section SI.3: Description of the data filtering rationale used for δD and $\Delta_{^{12}CH_2D_2}$ measurements on the 253 Ultra; Fig. SI.2 illustrating δD measurement and data processing in a flow-chart; Fig. SI.3 illustrating combined $\delta^{13}C$ and $\Delta_{^{13}CH_3D}$ measurement and data processing in a flow-chart; Fig. SI.4 illustrating $\Delta_{^{12}CH_2D_2}$ measurement and data processing in a flow-chart; Fig. SI.5 illustrating the convergence of PIMC PFRs as a function of the number of beads; Fig. SI.6 illustrating a comparison of the experiment *vs.* theory calibration of the present study to those published from other laboratories; Table SI.1: Convergence of PIMC PFRs as a function of the number of beads (data for Figure SI.5); Table SI.2: Individual analyses of methane isotope compositions of in-house reference standards; Table SI.3: Individual isotope analyses of methane from equilibration experiments; Table SI.4: Comparison between traditional BMU calculations and PIMC methods in δ notation; Table SI. 5: Theoretically calculated reduced partition function ratios (RPFRs) from both PIMC and BMU calculations derived from the complete partition function ratios (PFRs) presented in the main text;

Table SI.6: Harmonic vibrational frequencies of methane isotopologues derived from the potential energy surface of Lee and co-workers[34] used in the BMU calculations of the present study.

8. References

(1) Whiticar, M. .; Faber, E.; Schoell, M. Biogenic Methane Formation in Marine and Freshwater Environments: CO2 Reduction vs. Acetate Fermentation—Isotope Evidence. *Geochim. Cosmochim. Acta* **1986**, *50* (5), 693–709. https://doi.org/10.1016/0016-7037(86)90346-7.

(2) Whiticar, M. J. Carbon and Hydrogen Isotope Systematics of Bacterial Formation and Oxidation of Methane. *Chem. Geol.* **1999**, *161* (1–3), 291–314. https://doi.org/10.1016/S0009-2541(99)00092-3.

(3) Bernard, B. B.; Brooks, J. M.; Sackett, W. M. Natural Gas Seepage in the Gulf of Mexico. *Earth Planet. Sci. Lett.* **1976**, *31* (1), 48–54. https://doi.org/10.1016/0012-821X(76)90095-9.

(4) Chung, H. M.; Gormly, J. R.; Squires, R. M. Origin of Gaseous Hydrocarbons in Subsurface Environments: Theoretical Considerations of Carbon Isotope Distribution. *Chem. Geol.* **1988**, *71* (1–3), 97–104. https://doi.org/10.1016/0009-2541(88)90108-8.

(5) Stolper, D. A.; Sessions, A. L.; Ferreira, A. A.; Santos Neto, E. V.; Schimmelmann, A.; Shusta, S. S.; Valentine, D. L.; Eiler, J. M. Combined 13C-D and D-D Clumping in Methane: Methods and Preliminary Results. *Geochim. Cosmochim. Acta* **2014**, *126*, 169–191. https://doi.org/10.1016/j.gca.2013.10.045.

(6) Ono, S.; Wang, D. T.; Gruen, D. S.; Sherwood Lollar, B.; Zahniser, M. S.; McManus, B. J.; Nelson, D. D. Measurement of a Doubly Substituted Methane Isotopologue, 13 CH 3 D, by Tunable Infrared Laser Direct Absorption Spectroscopy. *Anal. Chem.* **2014**, *86* (13), 6487–6494. https://doi.org/10.1021/ac5010579.

(7) Young, E. D.; Kohl, I. E.; Lollar, B. S.; Etiope, G.; Rumble, D.; Li (李姝宁), S.; Haghnegahdar, M. A.; Schauble, E. A.; McCain, K. A.; Foustoukos, D. I.; et al. The Relative Abundances of Resolved L2CH2D2 and 13CH3D and Mechanisms Controlling Isotopic Bond Ordering in Abiotic and Biotic Methane Gases. *Geochim. Cosmochim. Acta* **2017**, *203*, 235–264. https://doi.org/10.1016/j.gca.2016.12.041.

(8) Ma, Q.; Wu, S.; Tang, Y. Formation and Abundance of Doubly-Substituted Methane Isotopologues (13CH3D) in Natural Gas Systems. *Geochim. Cosmochim. Acta* **2008**, *72* (22), 5446–5456. https://doi.org/http://dx.doi.org/10.1016/j.gca.2008.08.014.

(9) Liu, Q.; Liu, Y. Clumped-Isotope Signatures at Equilibrium of CH4, NH3, H2O, H2S and SO2. *Geochim. Cosmochim. Acta* **2016**, *175*, 252–270. https://doi.org/10.1016/j.gca.2015.11.040.

(10) Piasecki, A.; Sessions, A.; Peterson, B.; Eiler, J. Prediction of Equilibrium Distributions of Isotopologues for Methane, Ethane and Propane Using Density Functional Theory. *Geochim. Cosmochim. Acta* **2016**, *190*, 1–12. https://doi.org/10.1016/j.gca.2016.06.003.

(11) Webb, M. A.; Miller, T. F. Position-Specific and Clumped Stable Isotope Studies: Comparison of the Urey and Path-Integral Approaches for Carbon Dioxide, Nitrous Oxide, Methane, and Propane. *J. Phys. Chem. A* **2014**, *118* (2), 467–474. https://doi.org/10.1021/jp411134v.

(12) Giunta, T.; Young, E. D.; Warr, O.; Kohl, I.; Ash, J. L.; Martini, A.; Mundle, S. O. C.; Rumble, D.; Pérez-Rodríguez, I.; Wasley, M.; et al. Methane Sources and Sinks in

Continental Sedimentary Systems: New Insights from Paired Clumped Isotopologues 13CH3D and 12CH2D2. *Geochim. Cosmochim. Acta* **2019**, *245*, 327–351. https://doi.org/10.1016/j.gca.2018.10.030.

(13) Wang, D. T.; Reeves, E. P.; McDermott, J. M.; Seewald, J. S.; Ono, S. Clumped Isotopologue Constraints on the Origin of Methane at Seafloor Hot Springs. *Geochim. Cosmochim. Acta* **2018**, *223*, 141–158. https://doi.org/10.1016/j.gca.2017.11.030.

(14) Wang, D. T.; Gruen, D. S.; Lollar, B. S.; Hinrichs, K.-U.; Stewart, L. C.; Holden, J. F.; Hristov, A. N.; Pohlman, J. W.; Morrill, P. L.; Konneke, M.; et al. Nonequilibrium Clumped Isotope Signals in Microbial Methane. *Science (80-.).* **2015**, *348* (6233), 428–431. https://doi.org/10.1126/science.aaa4326.

(15) Stolper, D. A.; Lawson, M.; Davis, C. L.; Ferreira, A. A.; Neto, E. V. S.; Ellis, G. S.; Lewan, M. D.; Martini, A. M.; Tang, Y.; Schoell, M.; et al. Formation Temperatures of Thermogenic and Biogenic Methane. *Science (80-.).* **2014**, *344* (6191), 1500–1503. https://doi.org/10.1126/science.1254509.

(16) Stolper, D. A.; Martini, A. M.; Clog, M.; Douglas, P. M.; Shusta, S. S.; Valentine, D. L.; Sessions, A. L.; Eiler, J. M. Distinguishing and Understanding Thermogenic and Biogenic Sources of Methane Using Multiply Substituted Isotopologues. *Geochim. Cosmochim. Acta* **2015**, *161*, 219–247. https://doi.org/10.1016/j.gca.2015.04.015.

(17) Shuai, Y.; Etiope, G.; Zhang, S.; Douglas, P. M. J.; Huang, L.; Eiler, J. M. Methane Clumped Isotopes in the Songliao Basin (China): New Insights into Abiotic vs. Biotic Hydrocarbon Formation. *Earth Planet. Sci. Lett.* **2018**, *482*, 213–221. https://doi.org/10.1016/j.epsl.2017.10.057.

(18) Douglas, P. M. J.; Stolper, D. A.; Smith, D. A.; Walter Anthony, K. M.; Paull, C. K.; Dallimore, S.; Wik, M.; Crill, P. M.; Winterdahl, M.; Eiler, J. M.; et al. Diverse Origins of Arctic and Subarctic Methane Point Source Emissions Identified with Multiply-Substituted Isotopologues. *Geochim. Cosmochim. Acta* **2016**, *188*, 163–188. https://doi.org/10.1016/j.gca.2016.05.031.

(19) Douglas, P. M. J.; Stolper, D. A.; Eiler, J. M.; Sessions, A. L.; Lawson, M.; Shuai, Y.; Bishop, A.; Podlaha, O. G.; Ferreira, A. A.; Santos Neto, E. V.; et al. Methane Clumped Isotopes: Progress and Potential for a New Isotopic Tracer. *Org. Geochem.* **2017**, *113*, 262–282. https://doi.org/10.1016/j.orggeochem.2017.07.016.

(20) Stolper, D. A.; Lawson, M.; Formolo, M. J.; Davis, C. L.; Douglas, P. M. J.; Eiler, J. M. The Utility of Methane Clumped Isotopes to Constrain the Origins of Methane in Natural Gas Accumulations. *Geol. Soc. London, Spec. Publ.* **2018**. https://doi.org/10.1144/sp468.3.

(21) Inagaki, F.; Hinrichs, K. U.; Kubo, Y.; Bowles, M. W.; Heuer, V. B.; Hong, W. L.; Hoshino, T.; Ijiri, A.; Imachi, H.; Ito, M.; et al. Exploring Deep Microbial Life in Coal-Bearing Sediment down to 2.5 Km below the Ocean Floor. *Science (80-.).* **2015**, *349* (6246), 420–424. https://doi.org/10.1126/science.aaa6882.

(22) Ash, J. L.; Egger, M.; Treude, T.; Kohl, I.; Cragg, B.; Parkes, R. J.; Slomp, C. P.; Sherwood Lollar, B.; Young, E. D. Exchange Catalysis during Anaerobic Methanotrophy Revealed by 12CH2D2 and 13CH3D in Methane. *Geochemical Perspect. Lett.* **2019**, 26–30. https://doi.org/10.7185/geochemlet.1910.

(23) Eiler, J. M.; Clog, M.; Magyar, P.; Piasecki, A.; Sessions, A.; Stolper, D.; Deerberg, M.; Schlueter, H.-J.; Schwieters, J. A High-Resolution Gas-Source Isotope Ratio Mass Spectrometer. *Int. J. Mass Spectrom.* **2013**, *335*, 45–56.

https://doi.org/10.1016/j.ijms.2012.10.014.
(24) Young, E. D.; Rumble, D.; Freedman, P.; Mills, M. A Large-Radius High-Mass-Resolution Multiple-Collector Isotope Ratio Mass Spectrometer for Analysis of Rare Isotopologues of O2, N2, CH4 and Other Gases. *Int. J. Mass Spectrom.* **2016**, *401*, 1–10. https://doi.org/10.1016/j.ijms.2016.01.006.
(25) Wang, Z.; Schauble, E. A.; Eiler, J. M. Equilibrium Thermodynamics of Multiply Substituted Isotopologues of Molecular Gases. *Geochim. Cosmochim. Acta* **2004**, *68* (23), 4779–4797. https://doi.org/10.1016/j.gca.2004.05.039.
(26) Wilhelms, A.; Larter, S. R.; Head, I.; Farrimond, P.; Di-Primio, R.; Zwach, C. Biodegradation of Oil in Uplifted Basins Prevented by Deep-Burial Sterilization. *Nature* **2001**, *411* (6841), 1034–1037. https://doi.org/10.1038/35082535.
(27) Valentine, D. L. Emerging Topics in Marine Methane Biogeochemistry. *Ann. Rev. Mar. Sci.* **2011**, *3* (1), 147–171. https://doi.org/10.1146/annurev-marine-120709-142734.
(28) Hunt, J. M. *Petroleum Geochemistry and Geology*; W.H. Freeman, 1996.
(29) Bigeleisen, J.; Mayer, M. G. Calculation of Equilibrium Constants for Isotopic Exchange Reactions. *J. Chem. Phys.* **1947**, *15* (5), 261–267. https://doi.org/10.1063/1.1746492.
(30) Urey, H. C. The Thermodynamic Properties of Isotopic Substances. *J. Chem. Soc.* **1947**, 562. https://doi.org/10.1039/jr9470000562.
(31) Cao, X.; Liu, Y. Theoretical Estimation of the Equilibrium Distribution of Clumped Isotopes in Nature. *Geochim. Cosmochim. Acta* **2012**, *77*, 292–303. https://doi.org/10.1016/j.gca.2011.11.021.
(32) Richet, P.; Bottinga, Y.; Javoy, M. A Review of Hydrogen, Carbon, Nitrogen, Oxygen, Sulphur, and Chlorine Stable Isotope Fractionation among Gaseous Molecules. *Annu. Rev. Earth Planet. Sci.* **1977**, *5*, 65–110.
(33) Liu, Q.; Tossell, J. a.; Liu, Y. On the Proper Use of the Bigeleisen–Mayer Equation and Corrections to It in the Calculation of Isotopic Fractionation Equilibrium Constants. *Geochim. Cosmochim. Acta* **2010**, *74* (24), 6965–6983. https://doi.org/10.1016/j.gca.2010.09.014.
(34) Lee, T. J.; Martin, J. M. L.; Taylor, P. R. An Accurate Ab Initio Quartic Force Field and Vibrational Frequencies for CH 4 and Isotopomers. *J. Chem. Phys.* **1995**, *102* (1), 254–261. https://doi.org/10.1063/1.469398.
(35) Webb, M. A.; Wang, Y.; Braams, B. J.; Bowman, J. M.; Miller, T. F. Equilibrium Clumped-Isotope Effects in Doubly Substituted Isotopologues of Ethane. *Geochim. Cosmochim. Acta* **2017**, *197*, 14–26. https://doi.org/10.1016/j.gca.2016.10.001.
(36) Eldridge, D. L.; Lloyd, M. K.; Stolper, D. A. Methane Clumped Isotope Compositions From Ethane Pyrolysis Experiments. In *Goldschmidt Abstracts*; Barcelona, Spain, 2019.
(37) Turner, A. C.; Eldridge, D. L.; Bill, M.; Conrad, M. E.; Stolper, D. A. Experimental Calibration of Methane-H2-H2O Hydrogen Isotope Fractionation Factor from 4-160˚C. In *Goldschmidt Abstracts*; Barcelona, Spain, 2019.
(38) Wang, D. T.; Sattler, A.; Paccagnini, M.; Chen, F. G. Method for Calibrating Methane Clumped Isotope Measurements via Catalytic Equilibration of Methane Isotopologues on Γ-alumina. *Rapid Commun. Mass Spectrom.* https://doi.org/10.1002/rcm.8555.
(39) Yarnes, C. δ 13 C and δ 2 H Measurement of Methane from Ecological and Geological Sources by Gas Chromatography/Combustion/Pyrolysis Isotope-Ratio Mass Spectrometry. *Rapid Commun. Mass Spectrom.* **2013**, *27* (9), 1036–1044. https://doi.org/10.1002/rcm.6549.

(40) Larson, J. G.; Hall, W. K. Studies of the Hydrogen Held by Solids. VII. The Exchange of the Hydroxyl Groups of Alumina and Silica-Alumina Catalysts with Deuterated Methane. *J. Phys. Chem.* **1965**, *69* (9), 3080–3089. https://doi.org/10.1021/j100893a044.
(41) Robertson, P. J.; Scurrell, M. S.; Kemball, C. Exchange of Alkanes with Deuterium over γ-Alumina. A Brønsted Linear Free Energy Relationship. *J. Chem. Soc. Faraday Trans. 1 Phys. Chem. Condens. Phases* **1975**, *71*, 903. https://doi.org/10.1039/f19757100903.
(42) O'Neil, J. R. Theoretical and Experimental Aspects of Isotopic Fractionation. *Rev. Mineral.* **1986**, *16* (1), 1–40.
(43) Larson, J. G.; Hall, W. K. Studies of the Hydrogen Held by Solids. VII. The Exchange of the Hydroxyl Groups of Alumina and Silica-Alumina Catalysts with Deuterated Methane. *J. Phys. Chem.* **1965**, *69* (9), 3080–3089. https://doi.org/10.1021/j100893a044.
(44) Xie, H.; Formolo, M.; Lawson, M.; Eilier, J. Formation Mechanisms of Thermogenic Methane Revealed from 13CH3D and 12CH2D2 Measurements. In *International Clumped Isotope Workshop*; Long Beach, CA, 2019.
(45) Lloyd, M. K.; Eldridge, D. L.; Finnegan, S.; Dawson, T. E.; Stolper, D. A. Terrestrial Climate Records from Clumped Isotope Compositions of Wood Methoxyl Groups. In *AGU Fall Meeting*; San Francisco, California, 2019.
(46) Feynman, R. P.; Hibbs, A. R. *Quantum Mechanics and Path Integrals*; McGraw-Hill, 1965.
(47) Schweizer, K. S.; Stratt, R. M.; Chandler, D.; Wolynes, P. G. Convenient and Accurate Discretized Path Integral Methods for Equilibrium Quantum Mechanical Calculations. *J. Chem. Phys.* **1981**, *75* (3), 1347–1364. https://doi.org/10.1063/1.442141.
(48) Cheng, B.; Ceriotti, M. Direct Path Integral Estimators for Isotope Fractionation Ratios. *J. Chem. Phys.* **2014**, *141* (24), 244112. https://doi.org/10.1063/1.4904293.
(49) Tuckerman, M. E.; Berne, B. J.; Martyna, G. J.; Klein, M. L. Efficient Molecular Dynamics and Hybrid Monte Carlo Algorithms for Path Integrals. *J. Chem. Phys.* **1993**, *99* (4), 2796–2808. https://doi.org/10.1063/1.465188.
(50) Chacko, T.; Cole, D. R.; Horita, J. Equilibrium Oxygen, Hydrogen and Carbon Isotope Fractionation Factors Applicable to Geologic Systems. *Rev. Mineral. Geochemistry* **2001**, *43* (1), 1–81. https://doi.org/10.2138/gsrmg.43.1.1.
(51) Huntington, K. W.; Eiler, J. M.; Affek, H. P.; Guo, W.; Bonifacie, M.; Yeung, L. Y.; Thiagarajan, N.; Passey, B.; Tripati, A.; Daëron, M.; et al. Methods and Limitations of 'Clumped' CO 2 Isotope (Δ 47) Analysis by Gas-Source Isotope Ratio Mass Spectrometry. *J. Mass Spectrom.* **2009**, *44* (9), 1318–1329. https://doi.org/10.1002/jms.1614.

Table 1: Measurements of in-house reference standards including the comparison between conventional (UC Davis) and 253 Ultra measurements. All compositions reported in units of permil (‰). Assigned values for the house methane are in '*( )*'. σ = standard deviation.

	Conventional (UC Davis)							253 Ultra (UC Berkeley)														
Sample	*n*	δD_{VSMOW}	1σ[a]	1s.e.	$\delta^{13}C_{VPDB}$	1σ[b]	1s.e.	*n*	δD_{VSMOW}	1σ	1s.e.	$\delta^{13}C_{VPDB}$	1σ	1s.e.	$\Delta^{13}CH_3D_{(wg)}$*	$\Delta^{13}CH_3D$†	1σ	1s.e.	$\Delta^{12}CH_2D_{2(wg)}$*	$\Delta^{12}CH_2D_2$†	1σ	1s.e.	*n*
House	3	-159.3	2.4	1.4	-38.37	0.04	0.02	-	*(-159.3)*	-	-	*(-38.37)*	-	-	*(0)**	*(2.59)†*	-	-	*(0)**	*(5.86)†*	-	-	-
PlusD	2	-83.2	1.1	0.8	-38.34	0.14	0.10	9	-84.93	0.13	0.04	-38.37	0.03	0.01	-1.10	1.45	0.37	0.12	13.22	19.10	1.63	0.58	8
PlusD-200	2	20.0	0.1	0.1	-38.02	0.33	0.23	8	15.49	0.20	0.07	-38.33	0.01	0.00	-2.47	0.06	0.39	0.14	4.58	10.39	1.41	0.50	8
Plus^{13}C	2	-155.5	1.5	1.1	-5.26	0.22	0.16	4	-158.82	0.08	0.04	-5.82	0.02	0.01	4.56	7.16	0.09	0.05	1.73	7.60	0.26	0.15	3

[a]Typical external precision for δD-CH_4 measurements at UC Davis is ±4 ‰ (±1σ).

[b]Typical external precision for $\delta^{13}C$-CH_4 measurements at UC Davis is ±0.2 ‰ (±1σ).

*Compositions reported in the 'working gas reference frame' where the composition of the working gas ('house methane') is assumed to be $\Delta^{13}CH_3D = \Delta^{12}CH_2D_2 = 0$ ‰ (see Section 2.4.4).

†Compositions reported in the 'thermodynamic' reference frame where working gas ('house methane') is assigned $\Delta^{13}CH_3D = 2.59$‰ and $\Delta^{12}CH_2D_2 = 5.86$‰ based on the calibration provided in this study (see Section 4.1).

Table 2: Summary of equilibrated methane experiments. Compositions reported in units of permil (‰). σ = standard deviation.

T (˚C)	Catalyst	Duration (hr)	$\Delta^{13}CH_3D_{(wg)}$*	$\Delta^{13}CH_3D$†	1σ	1 s.e.	*n*	$\Delta^{12}CH_2D_{2(wg)}$*	$\Delta^{12}CH_2D_2$†	1σ	1 s.e.	*n*
500[a]	Ni	1 to 4	-1.82	0.76	0.23	0.06	16	-5.88	-0.06	1.92	0.64	9
400	Ni	4 to 6	-1.14	1.45	0.51	0.36	2	-2.39	3.45	0.40	0.28	2
350	Ni	9 to 12	-1.12	1.46	0.17	0.10	3	-2.41	3.44	-	1.21§	1
300	Ni	24 to 65	-1.33	1.26	0.16	0.11	2	-3.98	1.86	1.71	1.21	2
250[a]	Ni	72 to 184	-0.31	2.27	0.34	0.19	3	-0.85	5.00	2.48	1.43	3
165.4	γ-Al_2O_3	6.5 to 8.5	0.35	2.94	0.30	0.21	2	3.00	8.88	1.43	1.01	2
127.8	γ-Al_2O_3	23 to 25.5	0.77	3.36	0.11	0.08	2	3.76	9.64	0.58	0.41	2
75.7	γ-Al_2O_3	233 to 288	1.89	4.48	0.21	0.15	2	8.14	14.05	1.96	1.39	2
50.5	γ-Al_2O_3	292 to 478.5	2.49	5.09	0.24	0.17	2	8.18	14.09	0.46	0.33	2
25	γ-Al_2O_3	551 to 622	3.04	5.64	0.07	0.05	2	13.70	19.64	0.95	0.67	2
1.2	γ-Al_2O_3	503.5 to 816	4.42	7.02	0.09	0.06	2	17.54	23.50	1.54	1.09	2

[a]Note: Includes experiments performed with methane other than the 'house methane' (see Table SI.2 for a detailed listing).

*Reported in the 'working gas reference frame' where the composition of the working gas ('house methane') is assumed to be $\Delta^{13}CH_3D = \Delta^{12}CH_2D_2 = 0$ ‰ (see Section 2.4.4).

†Reported in the 'thermodynamic' reference frame where working gas is assigned $\Delta^{13}CH_3D = 2.59$‰ and $\Delta^{12}CH_2D_2 = 5.86$‰ based on the calibration of this study (see Section 4.1).

§In this instance, error is internal precision (±1 s.e.) because the value represents a single measurement.

Table 3: Results of PIMC calculations of equilibrium partition function ratios (PFRs)* and equilibrium constants (*K*).

		PFR_{PIMC}				PIMC					
T (˚C)	# of beads	$^{12}CH_3D/^{12}CH_4$	$^{13}CH_4/^{12}CH_4$	$^{13}CH_3D/^{12}CH_3D$	$^{12}CH_2D_2/^{12}CH_3D$	$K^{13}CH_3D$ †	$K^{12}CH_2D_2$ †	$1000\times\ln(K^{13}CH_3D)$ (‰)	1 s.e.	$1000\times\ln(8/3\times K^{12}CH_2D_2)$ (‰)	1 s.e.
-3.1	420	165.119	1.27411	1.28285	63.4149	1.006859	0.384056	6.836	0.028	23.86	0.33
1.2	414	156.615	1.27111	1.27953	60.1139	1.006620	0.383834	6.598	0.031	23.28	0.13
6.9	408	146.643	1.26726	1.27550	56.2243	1.006498	0.383409	6.477	0.021	22.18	0.22
16.9	396	131.403	1.26100	1.26863	50.2938	1.006054	0.382743	6.036	0.030	20.44	0.33
26.9	381	118.598	1.25512	1.26238	45.3268	1.005781	0.382190	5.764	0.029	18.99	0.26
36.9	372	107.730	1.24967	1.25649	41.1306	1.005456	0.381795	5.441	0.026	17.96	0.24
46.9	360	98.4964	1.24457	1.25106	37.5515	1.005215	0.381247	5.201	0.023	16.52	0.24
50.5	357	95.4660	1.24281	1.24914	36.3808	1.005094	0.381087	5.081	0.029	16.10	0.10
56.9	351	90.5717	1.23984	1.24598	34.4838	1.004946	0.380735	4.934	0.023	15.18	0.21
66.9	342	83.6501	1.23540	1.24118	31.8332	1.004682	0.380552	4.671	0.020	14.70	0.22
75.7	333	78.3302	1.23171	1.23723	29.7684	1.004477	0.380037	4.467	0.018	13.34	0.09
76.9	333	77.6800	1.23126	1.23680	29.5173	1.004494	0.379986	4.484	0.024	13.21	0.17
86.9	324	72.3917	1.22736	1.23258	27.4908	1.004256	0.379750	4.246	0.019	12.59	0.20
96.9	315	67.7750	1.22367	1.22864	25.7050	1.004062	0.379270	4.054	0.018	11.32	0.21
126.9	294	56.7170	1.21384	1.21810	21.4757	1.003510	0.378647	3.504	0.017	9.68	0.16
127.8	294	56.4316	1.21357	1.21781	21.3605	1.003489	0.378520	3.483	0.016	9.34	0.13
151.9	279	49.8849	1.20681	1.21059	18.8612	1.003128	0.378095	3.123	0.013	8.22	0.13
165.4	273	46.8367	1.20341	1.20696	17.6950	1.002952	0.377803	2.947	0.017	7.45	0.07
176.9	267	44.5391	1.20064	1.20402	16.8198	1.002813	0.377642	2.809	0.016	7.02	0.10
201.9	255	40.2836	1.19520	1.19822	15.1926	1.002525	0.377141	2.522	0.014	5.69	0.11
226.9	243	36.8111	1.19035	1.19309	13.8752	1.002306	0.376931	2.303	0.016	5.14	0.12
251.9	234	33.9564	1.18605	1.18848	12.7903	1.002045	0.376669	2.042	0.011	4.44	0.11
276.9	225	31.5734	1.18216	1.18436	11.8863	1.001869	0.376466	1.867	0.009	3.90	0.13
301.9	216	29.5629	1.17866	1.18065	11.1224	1.001685	0.376228	1.684	0.009	3.27	0.13
326.9	207	27.8446	1.17549	1.17729	10.4729	1.001537	0.376121	1.536	0.012	2.98	0.11
351.9	201	26.3684	1.17263	1.17427	9.91438	1.001400	0.375995	1.399	0.007	2.65	0.12
376.9	195	25.0874	1.16998	1.17148	9.42967	1.001289	0.375873	1.288	0.010	2.33	0.10
401.9	189	23.9686	1.16758	1.16894	9.00554	1.001169	0.375723	1.169	0.008	1.93	0.10
426.9	183	22.9861	1.16538	1.16663	8.63492	1.001067	0.375659	1.066	0.007	1.75	0.10
451.9	177	22.1140	1.16335	1.16448	8.30600	1.000966	0.375599	0.966	0.006	1.60	0.08
476.9	174	21.3370	1.16148	1.16252	8.01303	1.000893	0.375547	0.892	0.007	1.46	0.09
501.9	168	20.6483	1.15975	1.16071	7.75197	1.000828	0.375430	0.828	0.006	1.15	0.06
526.9	165	20.0243	1.15816	1.15903	7.51883	1.000752	0.375485	0.752	0.007	1.29	0.09

*See also Table SI.5 (Supplementary Information) where PFRs are converted into RPFRs in the conventional format.
†Note: $K^{12}CH_2D_2$ converges to 3/8 = 0.375 in the high temperature limit, whereas $K^{13}CH_3D$ converges to 1.

Table 4: Results of BMU calculations of equilibrium partition function ratios (PFRs)* and equilibrium constants (K).

	PFR_{BMU}				BMU			
T (°C)	$^{12}CH_3D/^{12}CH_4$	$^{13}CH_4/^{12}CH_4$	$^{13}CH_3D/^{12}CH_3D$	$^{12}CH_2D_2/^{12}CH_3D$	$K^{13}CH_3D$ †	$K^{12}CH_2D_2$ †	$1000\times\ln(K^{13}CH_3D)$ (‰)	$1000\times\ln(8/3\times K^{12}CH_2D_2)$ (‰)
-3.1	180.660	1.28108	1.28976	69.4098	1.006779	0.384201	6.757	24.24
1.2	171.175	1.27792	1.28637	65.7119	1.006611	0.383887	6.589	23.42
6.9	160.000	1.27397	1.28212	61.3595	1.006400	0.383498	6.380	22.41
16.9	142.909	1.26739	1.27506	54.7135	1.006050	0.382856	6.032	20.73
26.9	128.622	1.26129	1.26851	49.1685	1.005725	0.382271	5.709	19.20
36.9	116.567	1.25562	1.26243	44.4976	1.005424	0.381735	5.409	17.80
46.9	106.305	1.25033	1.25676	40.5283	1.005143	0.381245	5.130	16.52
50.5	102.938	1.24849	1.25479	39.2273	1.005046	0.381076	5.033	16.07
56.9	97.5017	1.24540	1.25148	37.1282	1.004882	0.380796	4.870	15.34
66.9	89.8940	1.24077	1.24653	34.1942	1.004638	0.380384	4.628	14.25
75.7	83.9921	1.23692	1.24241	31.9210	1.004436	0.380047	4.426	13.37
76.9	83.2758	1.23644	1.24189	31.6453	1.004411	0.380006	4.401	13.26
86.9	77.4829	1.23237	1.23754	29.4170	1.004197	0.379658	4.189	12.34
96.9	72.3835	1.22854	1.23345	27.4578	1.003997	0.379338	3.989	11.50
126.9	60.2730	1.21830	1.22252	22.8147	1.003468	0.378523	3.462	9.35
127.8	59.9524	1.21800	1.22221	22.6920	1.003452	0.378500	3.446	9.29
151.9	52.8184	1.21098	1.21472	19.9642	1.003093	0.377978	3.088	7.91
165.4	49.4964	1.20739	1.21091	18.6960	1.002912	0.377724	2.907	7.24
176.9	47.0036	1.20455	1.20788	17.7453	1.002769	0.377530	2.765	6.72
201.9	42.3752	1.19887	1.20185	15.9822	1.002485	0.377159	2.482	5.74
226.9	38.6264	1.19382	1.19649	14.5564	1.002237	0.376851	2.235	4.93
251.9	35.5440	1.18931	1.19171	13.3857	1.002019	0.376595	2.016	4.24
276.9	32.9760	1.18525	1.18742	12.4115	1.001825	0.376379	1.824	3.67
301.9	30.8116	1.18160	1.18355	11.5912	1.001654	0.376198	1.652	3.19
326.9	28.9685	1.17828	1.18005	10.8934	1.001501	0.376044	1.500	2.78
351.9	27.3848	1.17527	1.17688	10.2943	1.001365	0.375914	1.364	2.43
376.9	26.0127	1.17253	1.17398	9.77564	1.001243	0.375802	1.242	2.14
401.9	24.8153	1.17001	1.17134	9.32329	1.001134	0.375707	1.133	1.88
426.9	23.7634	1.16771	1.16892	8.92614	1.001036	0.375625	1.035	1.67
451.9	22.8338	1.16559	1.16669	8.57534	1.000948	0.375554	0.947	1.48
476.9	22.0077	1.16363	1.16464	8.26376	1.000868	0.375493	0.868	1.31
501.9	21.2700	1.16182	1.16275	7.98563	1.000796	0.375440	0.796	1.17
526.9	20.6082	1.16015	1.16099	7.73620	1.000731	0.375394	0.731	1.05

* See also Table SI.5 (Supplementary Information) where PFRs are converted into RPFRs in the conventional format.

† Note: $K^{12}CH_2D_2$ converges to 3/8 = 0.375 in the high temperature limit, whereas $K^{13}CH_3D$ converges to 1.

Table 5: Comparison between theoretical (PIMC) and experimental equilibrium clumped methane compositions as a function of temperature. Listing follows Table 2.

	PIMC	Experiment				PIMC	Experiment			
T (°C)	$1000\times\ln(K^{13}CH_3D)$*	$1000\times\ln(\Delta^{13}CH_3D/1000+1)$	1σ	1 s.e.	residuals	$1000\times\ln(8/3\times K^{12}CH_2D_2)$*	$1000\times\ln(\Delta^{12}CH_2D_2/1000+1)$	1σ	1 s.e.	residuals
500	0.82	0.76	0.23	0.06	-0.06	1.30	-0.06	1.93	0.64	-1.36
400	1.18	1.44	0.51	0.36	0.27	2.03	3.45	0.40	0.28	1.42
350	1.41	1.46	0.17	0.10	0.05	2.60	3.43	-	1.21§	0.83
300	1.70	1.26	0.16	0.11	-0.45	3.39	1.86	1.72	1.22	-1.52
250	2.07	2.27	0.34	0.20	0.20	4.47	4.99	2.49	1.44	0.52
165.4	2.95	2.93	0.30	0.21	-0.02	7.43	8.84	1.44	1.02	1.42
127.8	3.50	3.35	0.11	0.08	-0.14	9.46	9.59	0.59	0.42	0.14
75.7	4.48	4.47	0.21	0.15	-0.01	13.45	13.95	1.98	1.40	0.50
50.5	5.09	5.07	0.24	0.17	-0.01	16.08	13.99	0.47	0.33	-2.09
25	5.81	5.62	0.07	0.05	-0.19	19.36	19.45	0.95	0.67	0.08
1.2	6.64	7.00	0.09	0.06	0.36	23.15	23.23	1.55	1.10	0.08
1σ					***0.22***					***1.17***

*Computed from Eq. 10 or 11 in the main text (polynomial fits to PIMC calculations).

§In this instance, error is given as the internal precision (±1 s.e.) because the value represents a single measurement.

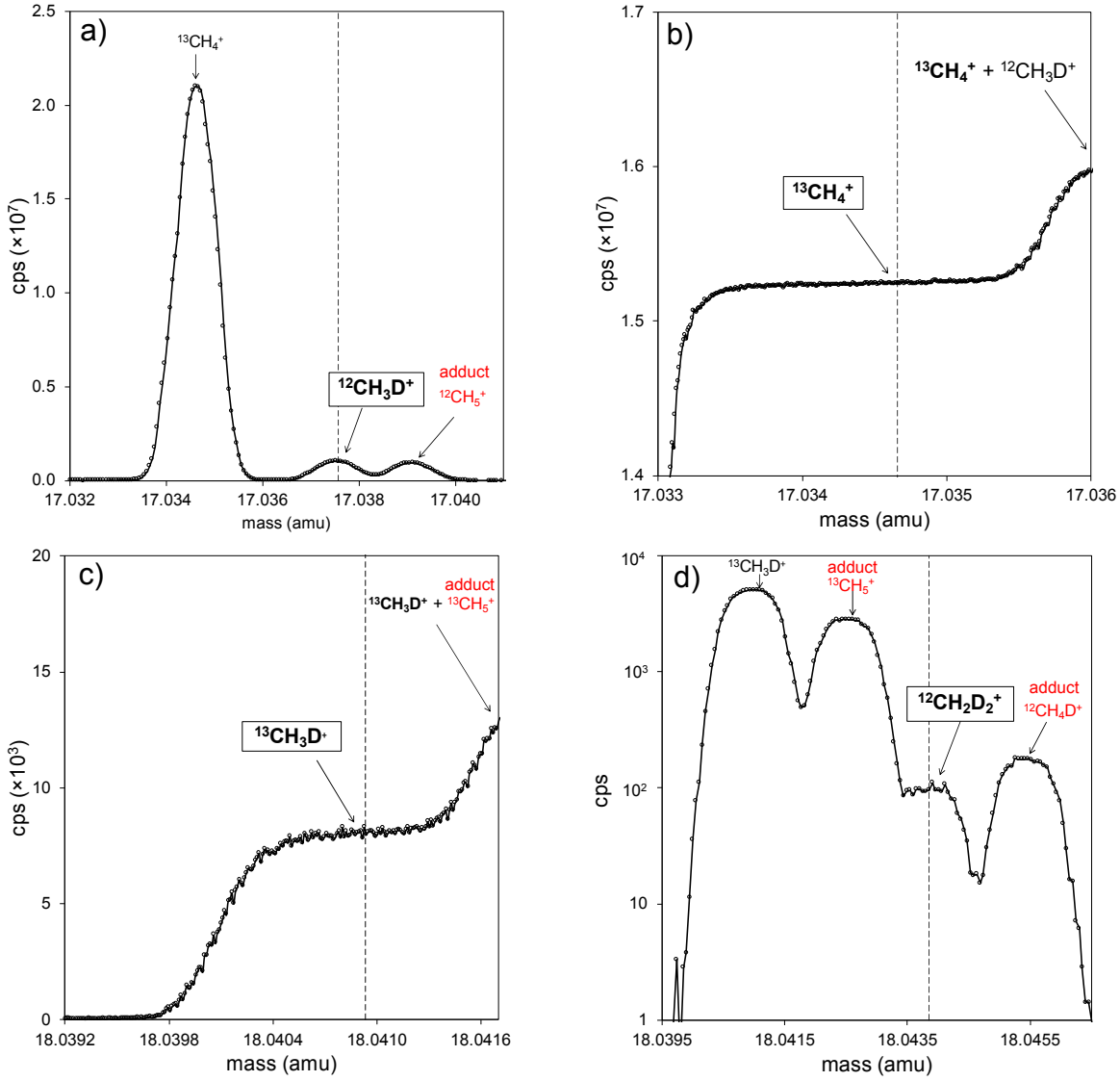

Figure 1(a-d): Mass scans performed under typical measurement conditions (cps = counts per second). Vertical dashed lines indicate where measurements are made. Boxed species are those that are measured and adducts are highlighted in red text (un-boxed species in black are other species/fragments). (a) mass-17 peaks; (b) flat $^{13}CH_4^+$ shoulder; (c) flat $^{13}CH_3D^+$shoulder; (d) mass-18 scan showing resolved $^{12}CH_2D_2^+$ (note the logarithmic scale of the y-axis for (d)).

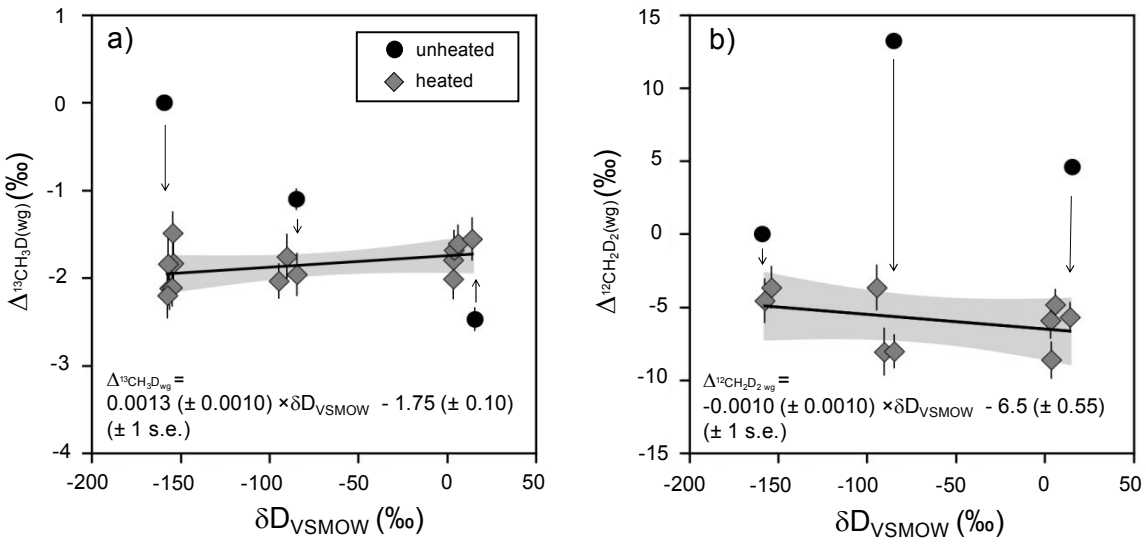

Figure 2(a-b): Measurements of $\Delta^{13}CH_3D_{(wg)}$ and $\Delta^{12}CH_2D_{2(wg)}$ as a function of δD_{VSMOW} values for 500˚C heated gas experiments. Black circles indicate the compositions of the starting gases (which correspond to the in-house reference standards). Grey diamonds represent the compositions measured after heating at 500˚C in the presence of Ni-based catalysts. All error bars are ±1 s.e. and reflect the internal precision of the individual measurements. A least-squares linear regression (black line, with grey 95% confidence intervals) yields no significant dependence of either $\Delta^{13}CH_3D_{(wg)}$ or $\Delta^{12}CH_2D_{2(wg)}$ on the δD_{VSMOW} of the gas.

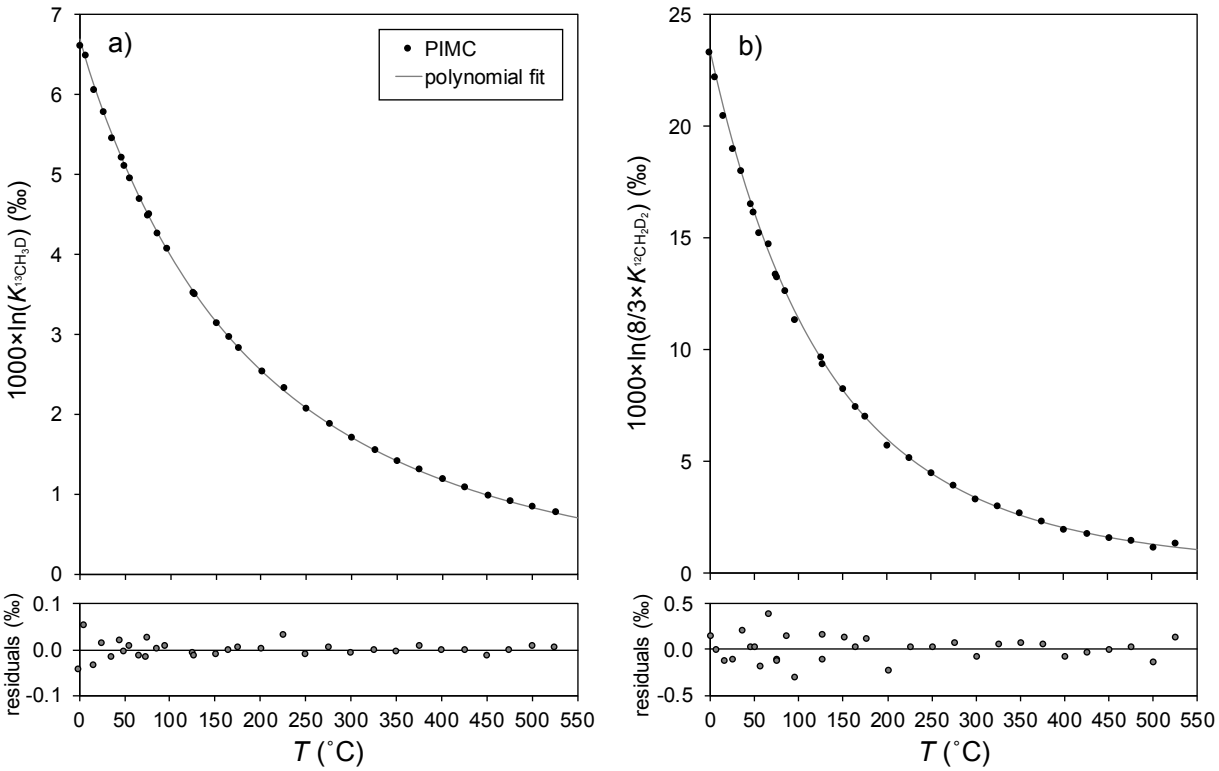

Figure 3(a-b): Results of PIMC calculations relative to the polynomial fits (Eq. 10 and 11) plotted as a function of temperature (see main text for further details). Error bars on PIMC calculations (±1 s.e.) are smaller than the data points.

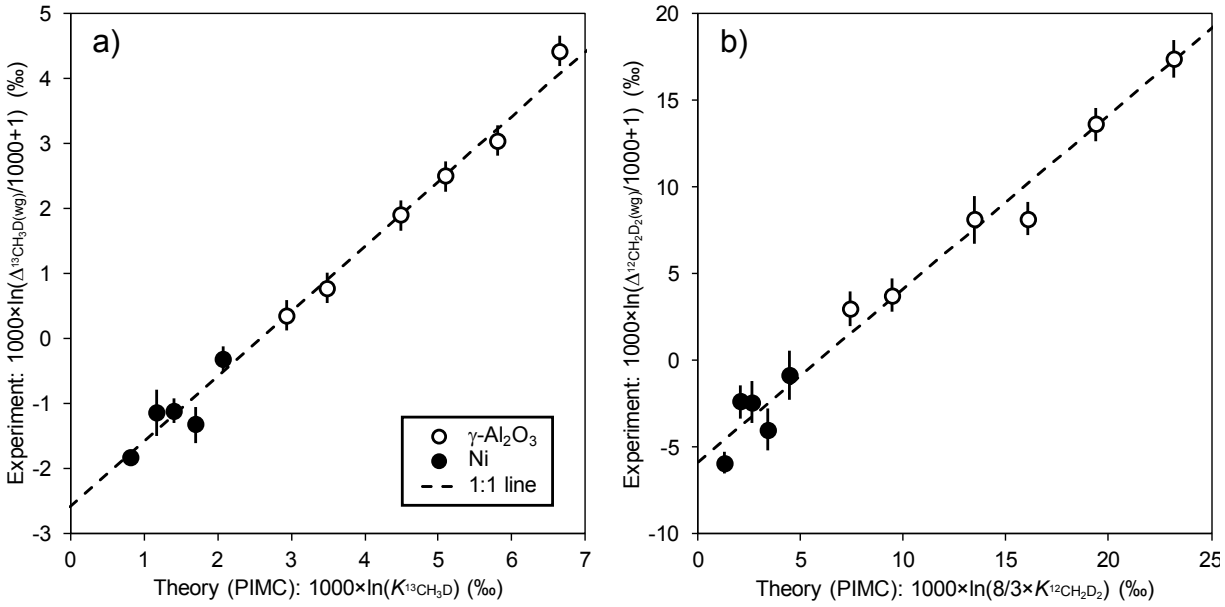

Figure 4(a-b): Comparison between theoretical and experimental calculations and measurements of methane clumping as a function of temperature: $1000\times\ln(\Delta_{(wg)}/1000+1)$ values from experiments (y-axis) *vs.* $1000 \times \ln\left(K_{^{13}CH_3D}\right)$ (panel (a)) and $1000 \times \ln\left(\frac{8}{3}K_{^{12}CH_2D_2}\right)$ values (panel (b)) theoretically computed from the PIMC calculations at the experimental temperatures (computed from Eq. 10 and 11) from 1-500˚C. Error bars for replicated experimental data points from this study represent either the ±1 s.e. of replicates (i.e., experimental reproducibility) or the expected ±1 s.e. based on the observed external precision of standards ($\sigma_{external}$) and the number of experimental replicates (i.e., $\sigma_{external}/\sqrt{n}$ where n = number of experimental replicates), whichever is larger. The error bar on one experimental data point from this study that has not been replicated (the $\Delta^{12}CH_2D_2$ value at 350˚C) represents ±1 s.e. internal precision (see Table 2). Error bars in the PIMC calculations (x-axis error bars, ±1 s.e.) are smaller than the symbols. Since experimentally measured values are shown in the 'working gas reference frame' (where the working gas is assumed to have $\Delta = 0$), the key aspect of this comparison is the relative difference between theory and experiment as a function of temperature. Experiments *vs.* theory are consistent with a 1:1 line (dashed) with respect to the temperature differences. The composition of the working gas can be constrained by interpolation (e.g., where the 1:1 dashed line intersects the x-axis) for the use of reporting measurements in the thermodynamic reference frame (absolute) represented by the PIMC calculations.

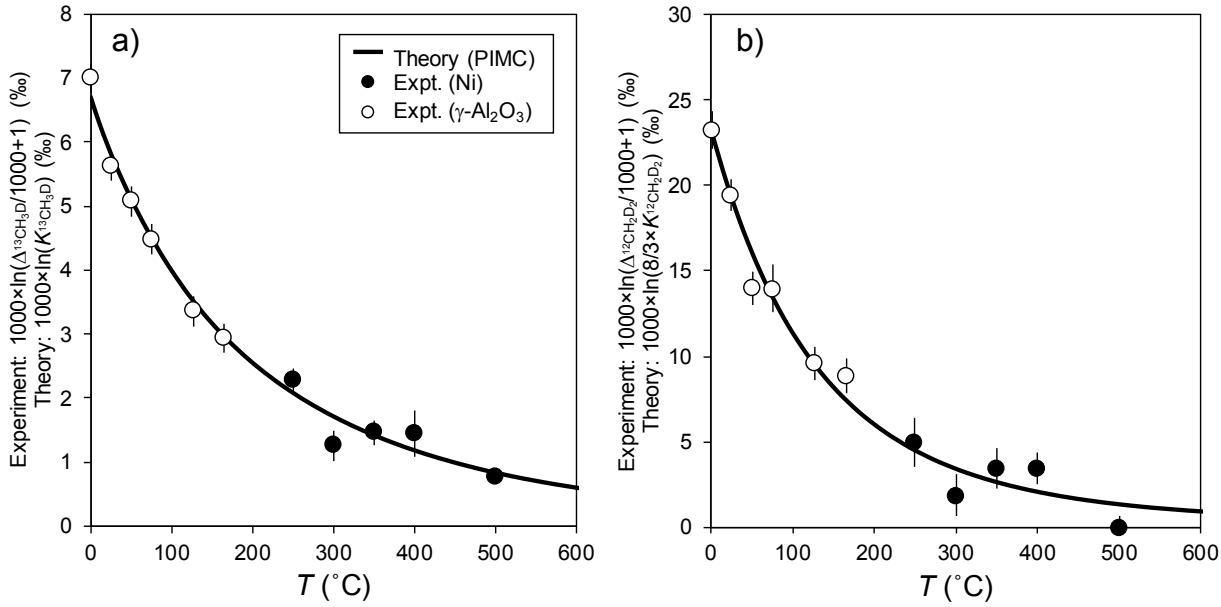

Figure 5(a-b): Plots of experimental *vs.* theoretical values of equilibrium clumping in methane as a function of temperature. Note that the theoretical calculations (black curves) are computed following Eq. 10 as $1000\times\ln(K_{^{13}CH_3D})$ values in (a) and following Eq. 11 as $1000\times\ln\left(\frac{8}{3}K_{^{12}CH_2D_2}\right)$ values in (b). Accordingly, the experimental data have been converted into the $1000\times\ln(\Delta/1000+1)$ format to facilitate direct comparison to theory (see also Table 5). Additionally, the experimental values are based on converting $\Delta_{(wg)}$ (reported in the 'working gas reference frame') into Δ values in the 'thermodynamic reference frame' by taking into consideration the constrained Δ compositions of the working gas ($\Delta_{^{13}CH_3D} = 2.59 \pm 0.14‰$ and $\Delta_{^{12}CH_2D_2} = 5.86 \pm 0.60‰$, ±1 s.e.; See Section 4.1). Error bars on experimental points are as described in Fig. 4.

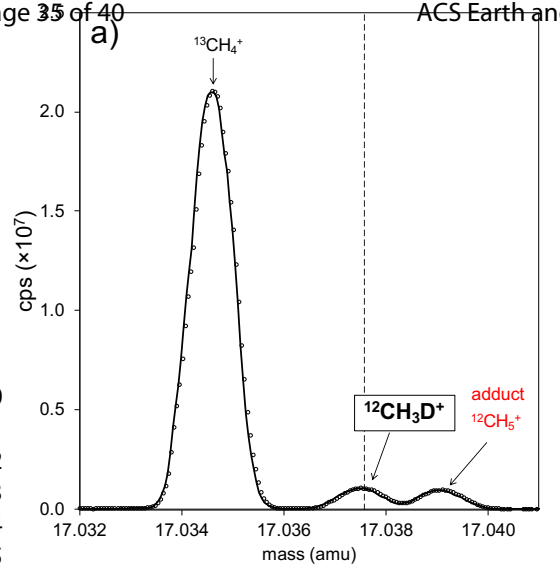

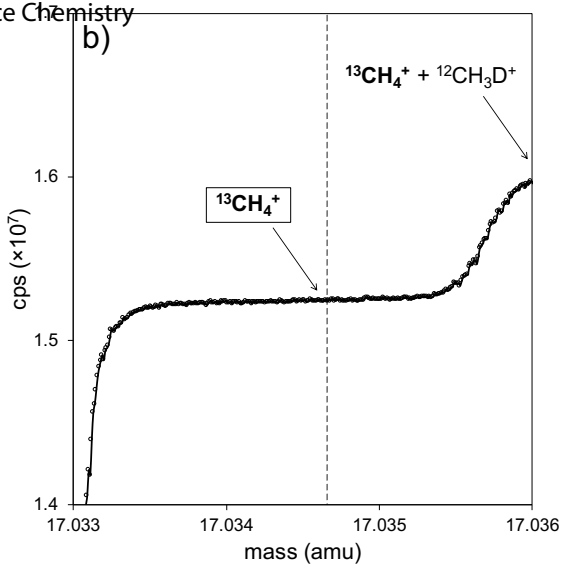

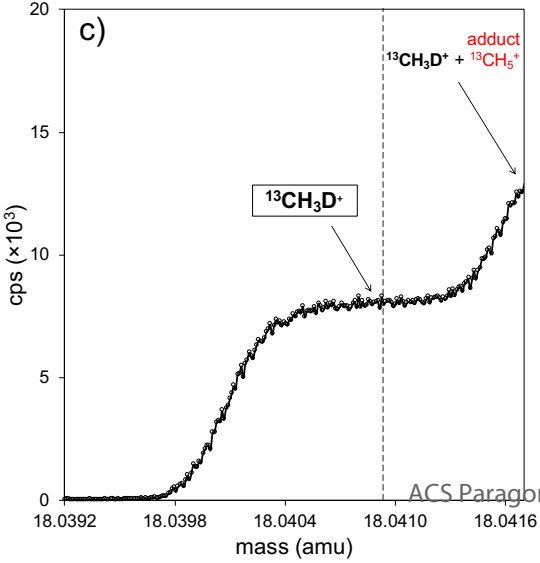

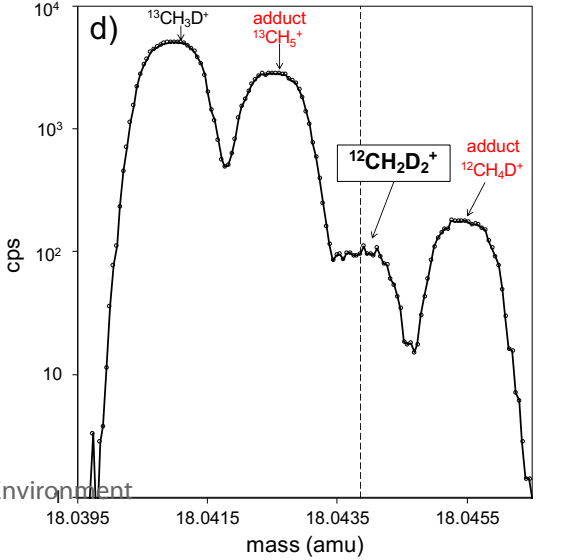

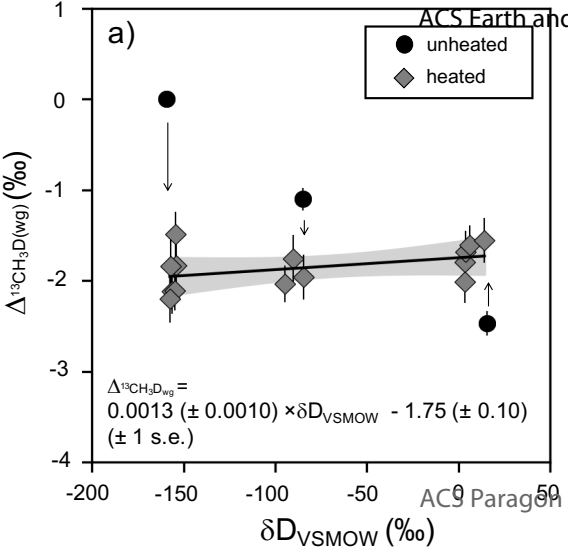

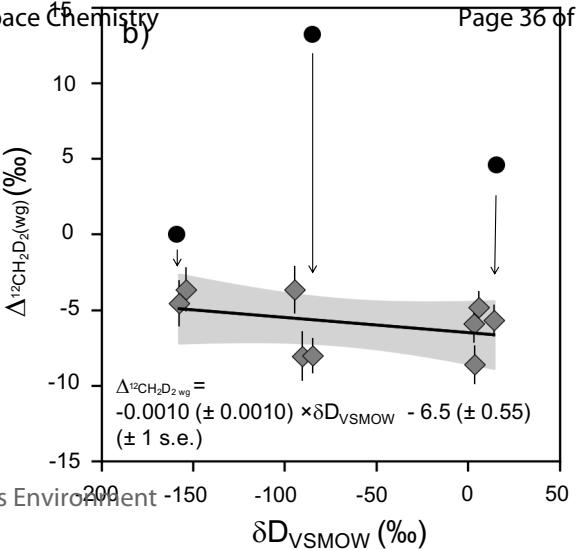

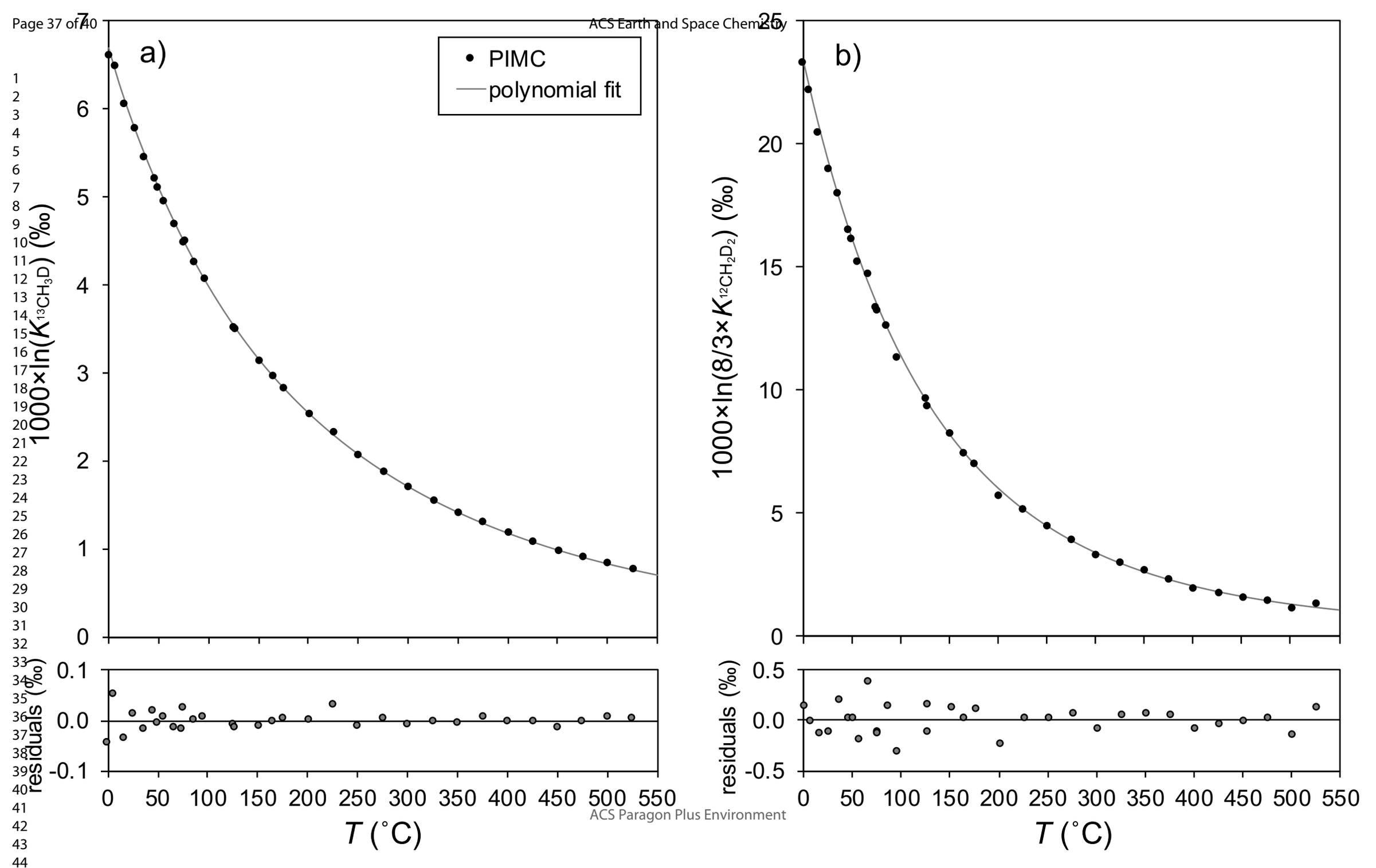
a)
PIMC
polynomial fit
1000×ln(K13CH3D) (‰)
residuals (‰)
T (˚C)
b)
1000×ln(8/3×K12CH2D2) (‰)
residuals (‰)
T (˚C)

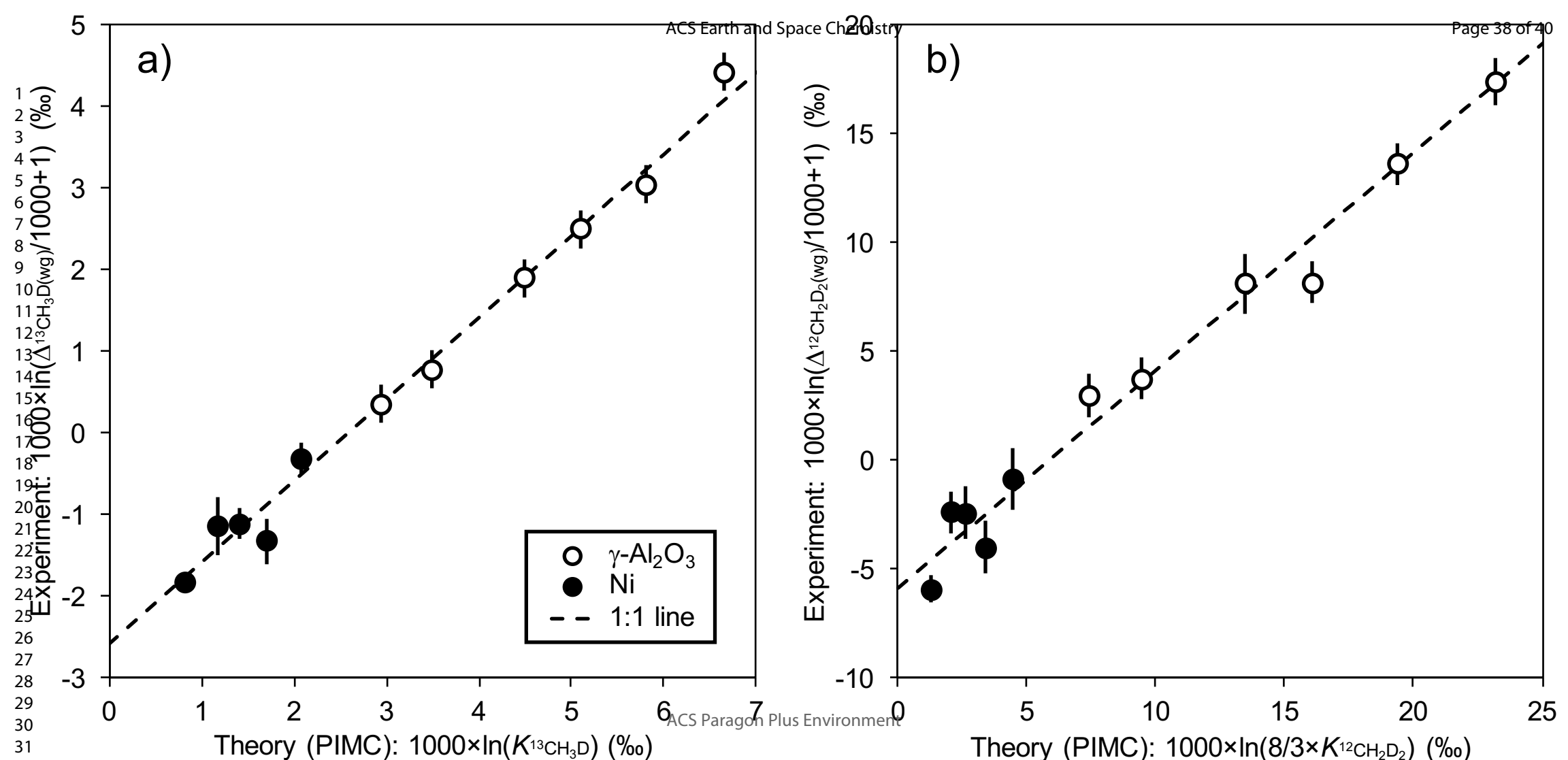
a)
b)
γ-Al2O3
Ni
1:1 line
Experiment: 1000×ln(Δ13CH3D(wg)/1000+1) (‰)
Theory (PIMC): 1000×ln(K13CH3D) (‰)
Experiment: 1000×ln(Δ12CH2D2(wg)/1000+1) (‰)
Theory (PIMC): 1000×ln(8/3×K12CH2D2) (‰)

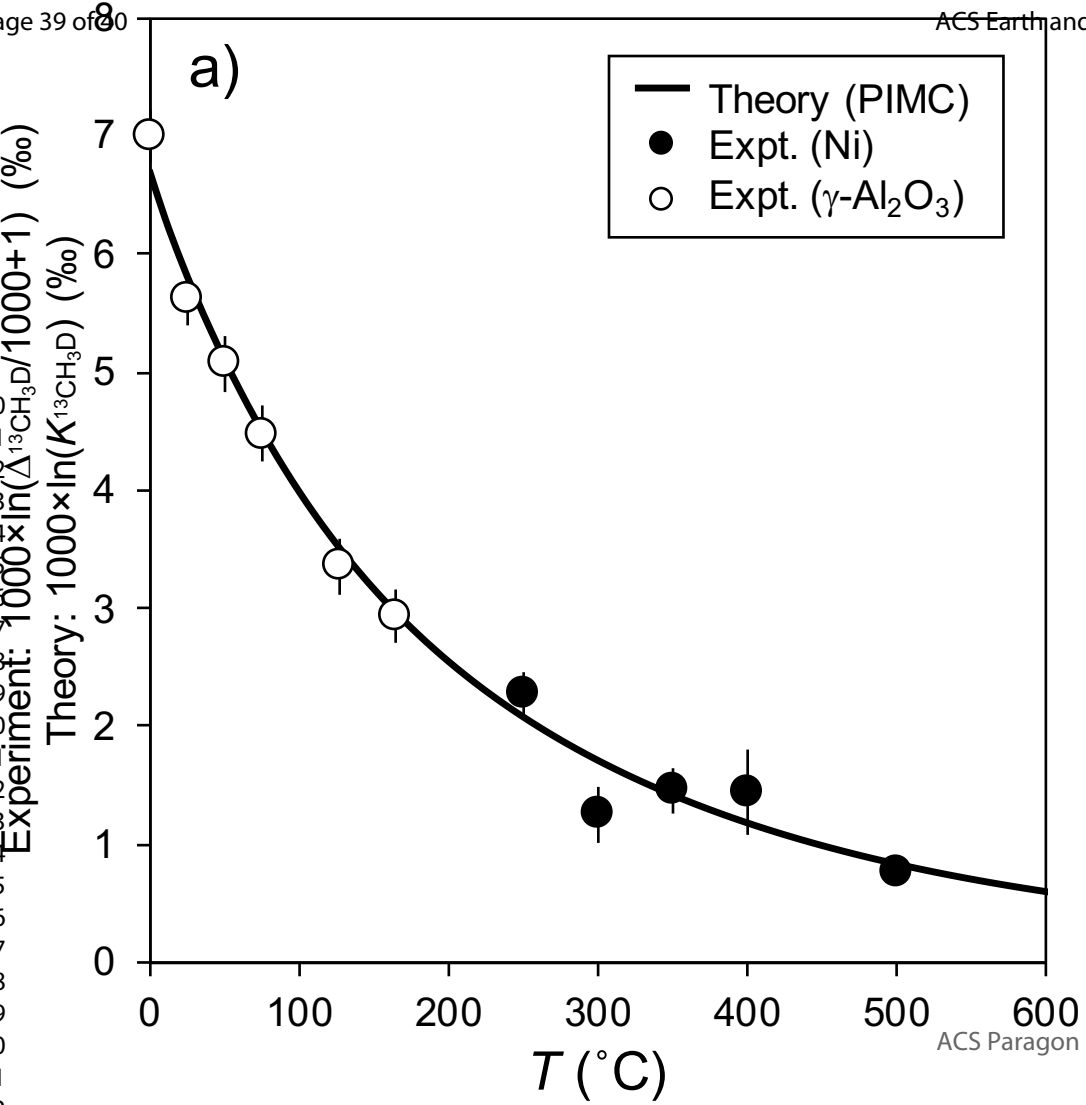
a)
Theory (PIMC)
Expt. (Ni)
Expt. (γ-Al2O3)
Experiment: 1000×ln(Δ13CH3D/1000+1) (‰)
Theory: 1000×ln(K13CH3D) (‰)
T (˚C)
0
100
200
300
400
500
600
0
1
2
3
4
5
6
7
8

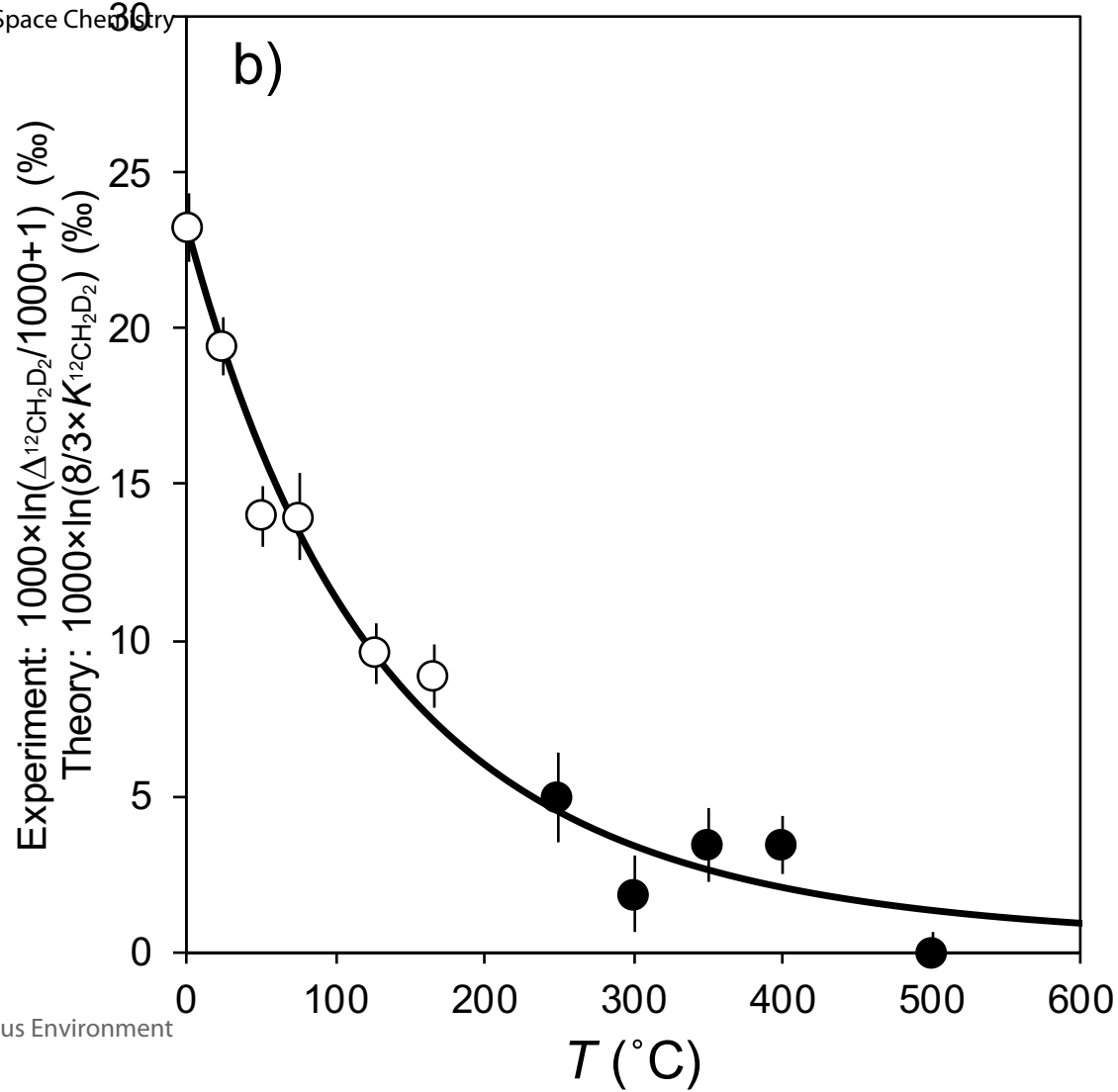
b)
Experiment: 1000×ln(Δ12CH2D2/1000+1) (‰)
Theory: 1000×ln(8/3×K12CH2D2) (‰)
T (˚C)
0
100
200
300
400
500
600
0
5
10
15
20
25
30